The Pennsylvania State University

The Graduate School

College of Earth and Mineral Sciences

ELECTROPHORETIC DEPOSITION: FUNDAMENTALS, MECHANISMS AND EXAMPLES WITH AN IN DEPTH EXAMINATION OF THE ION DEPLETION EFFECT

A Thesis in

Materials Science and Engineering

by

Jonathan J. Van Tassel

Submitted in Partial Fulfillment
of the Requirements
for the Degree of
Doctor of Philosophy

May 2004

ABSTRACT

The research and analysis for this thesis have been directed toward two major goals: to better understand the process of electrophoretic deposition (EPD) and to demonstrate its utility. This is also the order in which these two topics are addressed in the writing of this thesis.

In order to define the limits of the problem, the first chapter is devoted to a description and definition of what is, and is not, EPD. Here EPD is defined as consisting of three steps. The first is the creation of a charge balanced suspension of electrostatically charged particles in a solvent where some mechanism acts to keep the particles from floccing together during the time necessary to perform EPD. The second step is to create and maintain a DC electric field within the bulk of the solvent causing the electrostatically charged particles to move by electrophoresis toward an electrode. The final step is then to induce a change the nature of the suspension next to the electrode so that particles come into contact with each other and form a rigid deposition.

Chapter 2 then gives an outline of the scientific background necessary for understanding each of the three steps defined in Chapter 1. In order to make the complexity of the EPD system intellectually manageable, it is broken down into three components; solvent, particles, and electric field. Even though the scientific literature specifically on EPD is relatively modest, the literature on the binary interactions between each of these components (solvent-electric field, solvent-particle, etc.) is both extensive and elucidating. Previous reviews on EPD have concentrated almost exclusively on solvent-particle interactions. This thesis shows the vital importance of electrochemical reactions at the deposition electrode in understanding the mechanisms of deposition.

This approach also allows the categorization of mechanisms of EPD already demonstrated in the literature as well as the prediction of new mechanisms not previously demonstrated. To do this a list of mechanisms to prevent particles from floccing in the bulk suspension is compared to a list of effects that can be induced in the suspension at the deposition electrode. The list of specific near-electrode effects that can cause particles from specific types of suspensions to floc or coagulate at the electrode then becomes a list of the possible mechanisms of EPD. One of the most interesting of these mechanisms, ion depleted enhanced - automatic leveling deposition, was chosen for in-depth analysis.

The first step in this analysis is to obtain a complete understanding of the suspension from which the particles are to be deposited. This is done in Chapter 3 for alumina powder in ethanol with added HCl. Here it is shown that in the absence of dissolved ions alumina develops a significant positive surface charge in ethanol by the dissociative adsorption of ethanol molecules to the surface and the preferential desorption of ethoxide ions from the surface. The addition of HCl leads to a large rise in surface charge due initially to the reduction in ethoxide activity. After this initial rise the surface charge is set by a competitive adsorption equilibrium of chloride and ethoxide ions to positive surface sites on the powder.

Chapter 4 is then devoted to analyzing the deposition of alumina from this system. The first part of this chapter is detailed analysis of the conduction layer next to the cathode, the deposition electrode for the positively charged particles. The development of ionic and charge gradients, and the inevitability of a transition to convective transport at the electrode is shown for the electrolyte in the absence of particles. It is then shown that the dramatic change in conduction behavior in the presence of particles can be accounted for by the stabilization of an ion depleted, unbalanced charge conduction layer. Extremely high voltage gradients in this layer then exert a strong consolidating force on the positively charged alumina particles, compacting them into a densely packed deposited layer. This high gradient also leads to a strong equilibrating force to maintain a uniform thickness of the compact deposited layer, the automatic leveling effect.

The second objective here has been to demonstrate the potential utility of EPD in addressing current problems in the manufacture of electroceramic devices. This is undertaken in Chapter 5 with a complete description of the process to form suspensions, deposit particles, process these depositions into final form and to characterize the component created. The direct electrostatic deposition of silver/palladium powder is used to demonstrate the ability of EPD to create both very thin layers and very narrow conductor lines that can be measured on the scale of the particles used to create them. The electrophoretic deposition of PZT is used to demonstrate the formation of an intermediate thickness film with well controlled stoichiometry.

In the final chapter the thesis concludes with a discussion of what still needs to be done to advance the understanding and application of EPD.

TABLE OF CONTENTS

LIST OF FIGURES

LIST OF TABLES

Symbols used in Chapter 5

a	Particle radius (m)
c	Molar concentration of dissolved salt (Mol/dm^3)
e	Elementary charge (1.602E-19 C)
$\mathbf{E}$	Reduced electrophoretic mobility (non-dimensional)
h	Surface to surface separation distance
k	Boltzman Constant (1.381E-23 J/K)
q	Surface charge density (C/m^2)
r	Center to center particle separation distance
T	Temperature (K)
u_{E}	Particle electrophoretic mobility (μm·cm/V·s)
z	Ion valence
ε_o	Permittivity of free space (8.854E-12 C^2/J·m)
ε_r	Relative dielectric constant
ζ	Particle Potential at Shear Layer (mV)
$\tilde{\zeta}$	Reduced particle potential at shear layer (non-dimensional)
η	Solvent Viscosity (Poise)
κ	Inverse Debye length (m^{-1})
ρ_∞	Number density of dissociated molecules of a binary salt in bulk solution (m^{-3})

Chapter 5

Example Applications of Electrophoretic Deposition

5.1 Introduction

Chapter 2 was a purely theoretical discussion of the mechanisms of EPD. Chapters 3 & 4 were detailed analyses of an ideal system deliberately chosen for its simplicity. This chapter now leaves simplicity behind to offer specific case studies of the application of EPD to non-ideal materials. These case studies not only cover the deposition of the materials but devote an equal or greater consideration to the processing necessary to turn these depositions into useful structures. This is important firstly because demonstrating useful end products that would be difficult and/or expensive to produce by any other means demonstrates the value of EPD. Secondly, examining what needs to be done to a deposition to turn it into a useful product highlights what is important in the EPD process.

The first demonstration is the deposition of a silver/palladium powder. This includes an extended discussion of the electrostatic stabilization and EPD of the powder. This includes a short mention of two of the most significant problems in obtaining a uniform deposition of a metal powder, gravitational convection and ramified growth.

The second half of this section is then devoted to a discussion/demonstration of how these depositions can be incorporated into multilayer devices. The key point demonstrated here is that the minimum scale for EPD is the size of the individual particles. This means that EPD can take maximum advantage of reduced particulate sizes to produce the minimum thickness and feature sizes possible from a given particulate size starting material. This makes EPD the ideal technology for handling the very fine powders and producing the very thin layers that will be necessary for the fabrication of nano-scale composite devices.

The next section is devoted to the forming of intermediate thickness films of lead zirconate titanate (PZT) a piezoelectric ceramic. This begins with a description of some of the steps taken to find a suspension/deposition solvent system. This includes some experiments that, in hindsight, might lead to better deposition systems for the formation of these films than the one chosen. However, analysis of the chosen system, very low ionic strength glacial acetic acid, shows the mechanism for producing extremely low density depositions. There are many applications where this might be a significant advantage. If the deposition is allowed to dry normally then capillary forces will consolidate the deposition to close to maximum random packing density. The second half of this section is devoted to turning this packed particle coating into a dense continuous film, and evaluating the quality of that film in comparison to bulk samples of the same material.

Finally, the deposition of titania from acidified ethanol is discussed. The main point of this section is to highlight the advantage of the automatic leveling behavior of the ion depletion enhanced deposition mechanism compared to the direct electrostatic deposition mechanism.

5.2 Silver/Palladium Deposition

For nearly fifty years multilayer ceramic structures have been fabricated by casting a continuous ceramic tape, screen printing a patterned electrode layer onto the tape, stacking the tape layers and lamination of these multicomponent tapes. This is followed by de-binding and sintering to form devices such as multilayer ceramic capacitors and multilayer co-fired ceramic (MLCC) substrates and wiring modules. As with all electronic devices, there is continuous pressure to reduce device sizes and increase volumetric efficiency. The state of the art is being pushed fastest in the multilayer capacitor industry where commercial devices currently available have 2 μm dielectric layers separating 0.5 μm electrode layers, with the near term target to reduce these thicknesses to one micron and a few hundred nanometers respectively. Aiding this drive to sub-micron feature sizes is an increasing availability of ceramic and metal powders in the nanometer size range. It is unclear at this point if tape casting and screen printing will be able to take advantage of these nano powders to produce the sub-micron features necessary for future devices. It is therefore important to consider and demonstrate new methods to take particulate processing into the nanoparticle age.

Unlike the deposition in Ch. 4, this is an example of an EPD system with minimal accompanying electrolytic conduction. While this does not eliminate electrochemical effects, analysis of the particles' electrostatic stabilizing force suggest that in this case deposition can be explained by the simple electrostatic force on a charged particle in the applied electric field.

This, arguably the simplest of the EPD mechanisms, allows particles to be brought into the deposition uniformly from their random distribution in the bulk suspension. The random addition of individual particles to the deposition allows the formation of extremely uniform thin particulate layers. As is shown below, layers of particles deposited by EPD only two to three particle diameters thick can be consolidated and sintered to form dense, continuous layers in a multilayer structure.

5.2.1 Materials

Deposited Powder — The powder used is a 70/30 alloyed silver/palladium composition (EGAG07001 from PGP Industries, Inc. Santa Fe Springs, California.) The particles are spherical with an average diameter of 0.3 μm as determined by light scattering (MasterSizer, Malvern Instruments, United Kingdom). The surface area is 1.73 m^2/g as determined by single point BET (Monosorb MS-12, Quantachrome) giving an equivalent surface area diameter of 0.32 μm.

Acetic Acid — J. T. Baker glacial acetic acid, 99.5-100.5%, (J. T. Baker Co., Phillipsburg, New Jersey.) was used as the suspending solvent.

Deposition Substrates — Deposition was conducted onto three types of substrates - Pre-sintered alumina substrates (Superstrate 996, Coors Ceramics Co., Golden, CO), glass, and polyester film. The conductive deposition electrode on all three substrates was created by a sputtered platinum coating of ≈ 40 nm thickness. Patterns on glass substrates were created by scribing a continuous coating. Patterns on polyester film substrates were created using an UV-photolithographic mask on the film surface.

Pre-formed Ceramic Tapes — Laminations were carried out on pre-formed ceramic tapes. These include a commercially produced tape, DuPont LTCC tape 951-A, and tapes made in-house by Bi-coating Cabot hydrothermal $BaTiO_3$ powder (BT-8, Cabot Performance Materials, Boyertown, PA), (**1**) and mixing the powder with binder and solvent to form a slip, which was cast into tape by traditional methods.

5.2.2 Experimental Procedure

Suspension— Suspensions were produced by the addition of 1.0 g of powder to approximately 100g glacial acetic acid having a conductivity of less than 0.03μS/cm prior to the addition of the powder. The powder was then dispersed by sonication using a Branson Sonifier 350 at 70% setting for two minutes while stirring.

Mobility — Mobility was measured using a Delsa 440 laser Doppler velocimeter (Beckman Coulter, Inc., Fullerton, California). This instrument measures particle velocity in suspension within a rectangular capillary measuring 0.98 mm high, 3.17 mm wide, and 5.18 mm long. To separate the electro-osmotic flow of the fluid in the capillary from the electrophoretic motion of the particles, particle velocity was measured at nine points across the capillary, the results fitted to a parabola, and the particle velocities at the theoretical stationary levels calculated from the fitted parabola. The theoretical stationary layers at the center of the width of this capillary occur at 16% of the capillary height away from the top and bottom of the capillary. This is similar to the procedure outlined by Pelton et al. (**2**).

The measurement for each point from top to bottom of the capillary consisted of applying a constant voltage in one direction for two seconds, a one second interval, followed by application of the voltage in the opposite direction for two seconds. This is repeated for a total of 30 seconds. This is intended to minimize the voltage drop due to electrochemical polarization at the electrodes.

For a significant signal to be generated by the instrument the laser must be able to propagate across the capillary with only modest scattering. This requires that the sample have a volume density of particles in suspension of approximately 0.01%, one tenth the volume density of the deposition suspensions used here. To prepare these dilutions the suspension was allowed to sediment overnight yielding a clear supernatant. Some of this supernatant was removed, the particles re-suspended, and the suspension and supernatant mixed to yield the appropriate suspension density for measurement.

Conductivity — Conductivity was measured using an open sided, rectangular, parallel plate conductivity cell having a cell constant of 0.107 cm^{-1} (Thermo Orion, Beverly, Massachusetts). The voltage across the conductivity cell was measured using a voltage divider circuit. A 10 Hz sine wave input signal of ≈ 1V rms was provided by an HP 33120A signal generator. The voltage across the conductivity cell was reduced to ≈ 0.5 V rms using a resistance decade box. The total input voltage and voltage across the decade box were measured using an HP 54645A oscilloscope and used to calculate the resistance across the conductivity cell. This setup was calibrated over the range from 1 to 60 μS/cm by titration of KCl in water using the equation of Lind et al. (**3**) as standard.

Deposition — The powder was deposited onto a platinum electrode surface sputtered onto either a glass plate, for the overcasting demonstration, or onto 2.54 cm square pieces of uncoated polyester film tape casting carrier for the lamination demonstrations. The suspension was placed in a beaker with a gold foil in the bottom to serve as the anode. The deposition surface is held horizontally one half, one or two centimeters above the anode. The particles are then deposited vertically upward to get a deposition that is only due to electrophoretic effects without sedimentation components.

To deposit the particles an electric field of ≈ 300V/cm was applied. For the thinnest depositions the field was pulsed on and off in three or five second intervals to allow electroconvective circulation to dissipate. This was done to maximize the thickness uniformity of these very thin depositions. After deposition was complete, the substrate was removed from the holder and immediately rinsed by dipping and moving back and forth gently in as-received acetic acid. This is to remove any particles which are not deposited but are carried out of the deposition bath in the wetting film of acetic acid on its surface.

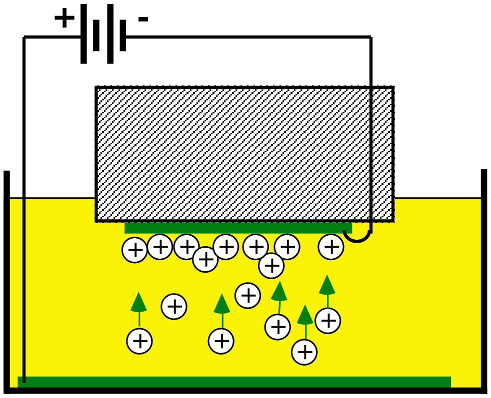

Fig. 5.1 Upward deposition separates EPD from sedimentation.

5.2.3 Dispersion and Deposition Results and Discussion

Electrophoretic Mobility — Several mobility measurements were made at voltage settings of 15, 30, 45, and 60 V. The measured mobility increased linearly by ≈ 20% from 15 to 60 V. This is presumably due to electrode polarization and therefore the mobility at the highest voltage was taken as the most accurate. One measurement at 60 V is shown in fig. 4. The parabola was fitted to the data by least squares. The r^2 fit of the parabola was 0.996. The mobility at the theoretical stationary levels is 0.25 μm·cm/V·s. Reproducibility of measurements was ± 5%. Suspensions with the conductivity reduced by dilution with fresh acetic acid had a mobility ≈ 10% less than the suspensions diluted only with suspension supernatant. Mobilities in the freshly prepared suspension and in the suspension after a series of depositions were estimated at 0.23 and 0.25 μm·cm/V·s respectively.

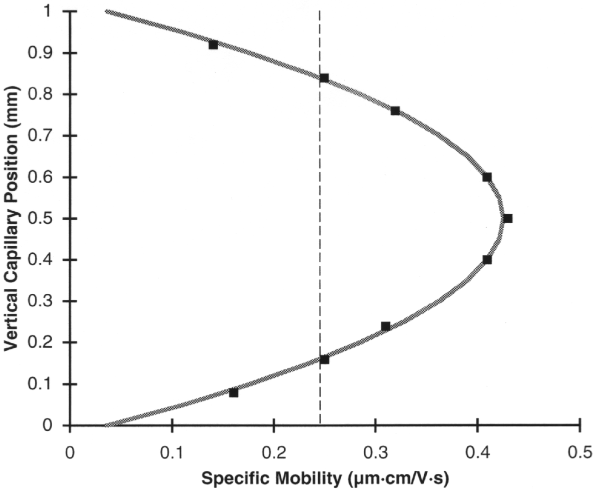

Fig. 5.2 Specific mobility vs. vertical position in measurement capillary. Vertical dashed line intersects parabola at theoretical stationary layers.

Conductivity and Ionic Strength — The conductivity of one typical suspension after sonication was 0.04 μS/cm. This conductivity increased with each deposition, presumably due to the electrolytic formation of ionizable species during conduction. After a total current flux through the suspension of 80 mC over the course of eighteen depositions the conductivity was 0.11 μS/cm. The conductivity measurements were reproducible within ±0.01 μS/cm, however, absent standardization for the range below 1 μS/cm, the absolute conductivity values here should be considered only approximate. Based on prior experience we believe that the measured values will be within a factor of two of the actual values.

In order to estimate the ionic content of the suspension without knowing the specific ionic species leading to conduction, it is necessary to make some assumptions. First, due to the low dielectric constant of acetic acid, it is assumed that any free ions will be univalent. Second, an approximate molar conductivity of 6 μScm^{-1}mMol^{-1} is chosen. This number is based on the work of B. V. Weidner who measured molar limit conductivities of various ammonium and nitrate salts ranging from 5 to 8 in pure acetic acid. [8] Using this value for the ionic molar conductivity it is possible to estimate the ionic content of the suspension as ranging from 6 μMol before deposition, rising to 18 μMol after a series of depositions.

In this series of eighteen depositions averaging twenty seconds each, a total current of 80 mC passed through the suspension. If the conduction does occur by an electrolytic process which produces an ion pair for each electron passing through the solution, this current would result in an increase of ionic content of 9 μMol in the 90 cc of this suspension. This is well within the error limits of the 12 μMol rise in the ionic concentration estimated by conductivity. Therefore, this hypothesis cannot be rejected.

With an estimate for the ionic strength of the solution it is now possible to calculate the inverse Debye length using eq. [5.1] for a solution containing univalent ions. (symbols used are defined in appendix.)

$$\kappa = \left[\frac{2e^2\rho_\infty}{\varepsilon_o\varepsilon_r kT}\right]^{\frac{1}{2}} \qquad \text{Inverse Debye Length} \qquad [5.1]$$

Ionic concentrations in the bulk solution, c of 6 and 18 μMol will yield Debye lengths, κ^{-1}, of 35 and 20 nm in acetic acid with a relative dielectric constant, ε_r, of 6.2. For the 300 nm particles used here this yields non-dimensional double layer thickness parameters, κa, of 4.3 and 7.5.

Surface potential and Surface Charge — With the particle electrophoretic mobility and the double layer thickness parameter it is possible to estimate the zeta potential of the particle. Unfortunately, the κa values here are within the range of 1 - 10 where the simple

Hückel and Smoluchowski formulae are not valid, and the non-dimensional electrophoretic mobility values, **E**, are 2.6 and 2.8, well outside of the 0 to 1 range for validity of the slightly more complex Henry formulation. (**5**, ch. 3)

$$\mathbf{E} = \frac{3\eta e}{2\varepsilon_r \varepsilon_o kT} u_E \qquad \text{Non-dimensional Electrophoretic Mobility} \qquad [5.2]$$

Therefore to estimate the surface potential, graphic interpolation of the charts published by O'Brien and White was used. (**6**) These calculations include the retardation due to polarization of the diffuse layer around the particle. These charts were calculated on the basis of KCl in water, where the ionic mobility is much higher than in the acetic acid suspension used here. The boundary layer polarization is likely to be higher in the suspension with the lower ionic mobility, leading to an under estimate of the of the actual surface potential. For E = 2.6 and 2.8, and κa's of 4.3 and 7.5, the non-dimensional surface potentials, $\tilde{\zeta}$, are both 3.0. This yields a constant surface potential of 77 mV independent of the solution ionic concentration.

$$\tilde{\zeta} = \frac{e\zeta}{kT} \qquad \text{Non-dimensional Surface Potential} \qquad [5.3]$$

With the surface potential and κa, the surface charge density can be calculated using the empirical formula of Loeb, et al. (**7**) for a 1-1 electrolyte system, eq. [5.4]. This gives a particle surface charge density, q, of 0.20 and 0.32 milliCoulombs/meter^2 for the 6 and 18 μMolar suspensions respectively. For the 300 nm particles here, this gives a total particle charges are 5.5 x 10^{-17} and 9.1 x 10^{-17} Coulombs.

$$q = \frac{\varepsilon_o \varepsilon_r kT}{e} \kappa \left(2\sinh\left(\tfrac{1}{2}\tilde{\zeta}\right) + \frac{4}{\kappa a} \tanh\left(\tfrac{1}{4}\tilde{\zeta}\right) \right) \qquad \text{Surface Charge Density} \qquad [5.4]$$

Stability — To prevent the particles from floccing and sedimenting out of the suspension prior to deposition there must be an adequate force to keep them apart. The force drawing them together is, of course, the London-Van der Waals force and, in this case, the force that must overcome this attraction is the increased osmotic pressure due to the compression/overlap of the particles diffuse counter-ion layers.

The L-VdW attraction between two particles is the product of two terms. The Hamaker Constant, which is a function of the electronic properties of the materials, and a geometric term defined by the arrangement of the materials. This is expressed in eq. [5.5] where A_{131} is the Hamaker constant and the balance is the geometric factor for spheres of radius a at a center to center separation distance of r. (**8** § 5.2)

$$\Phi = -A_{131} \frac{1}{6} \left(\frac{2a^2}{r^2 - 4a^2} + \frac{2a^2}{r^2} + \ln \frac{r^2 - 4a^2}{r^2} \right) \qquad [5.5]$$

L-VdW Interaction Energy for Two Spheres

For the Hamaker constant at zero separation we have used the value calculated by Parsegian and Weiss (**9**) for two masses of silver metal separated by water, $A_{131}(0) = 4.0\text{x}10^{-19}$ Joule. Given that silver and palladium form a full solid solution, it is reasonable to expect that the electronic properties of silver palladium will be similar to those of pure silver. Likewise, the close match of the optical frequency refractive indices for water and acetic acid, at 1.333 and 1.372 respectively, indicate that they will likely have a similar dielectric relaxation behavior in the UV range where all of the interaction takes place. These assumptions are supported by the approximation methods of Israelachvilli and their comparison to experimental values. (**10** § 11.4)

The Hamaker constant itself is a function of separation distance. The synchronization of dipole motions that leads to the London electrostatic attraction decays as the separation approaches a significant fraction of the length of the electromagnetic wave mediating this interaction. For the silver palladium particles here the interaction will be in the plasmon frequency range, ≈ 3 x 10^{15} s^{-1}, with a wavelength of 100 nm. This retardation effect leads to a decrease in the effective Hamaker constant by 50% at a separation distance of 10 nm and with the interaction almost completely disappearing at 100 nm. This retardation was calculated here using the method of Russel, et al. (**8** §5.9, 5.10)

The repulsive force was then calculated using the linearized Derjaguin approximation for two spheres at constant surface potential, eq. [5.6]. (**8** §4.10)

$$\Phi = 2\pi\varepsilon_r\varepsilon_o\zeta^2 a\ln\left(1+e^{-\kappa h}\right) \quad \text{Derjaguin Approx. Repulsion Energy} \qquad [5.6]$$

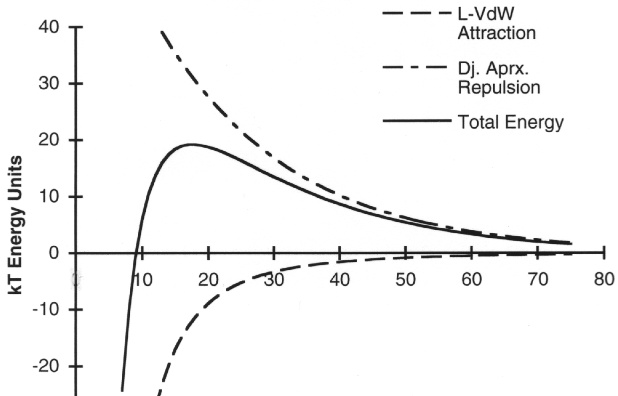

Fig. 5.3 Interaction potential for two 300 nm dia. silver palladium spheres in acetic acid; c = 18μMol.; Ψ_0 = 77 mV.

Summing the L-VdW and electrostatic interaction potentials gives the total interaction energy. This is shown in fig. 5.3 for the particles at the higher ionic strength condition. The calculated energy barrier to flocculation is 33 and 19 *kT* energy units and the maximum repulsion force is 2.6 x 10^{-12} N and 2.3 x 10^{-12} N for the 6 and 18 μMolar conditions respectively.

For the surface potentials found here, the linearization assumption in the Derjaguin approximation, eq. [5.6] of the electrostatic force will lead to an underestimation of the potential drop near the particle surface and therefore an overestimation of the energy barrier to flocculation and interparticle repulsive force. This may, at least in part, be compensated by a likely underestimation of the surface potential above.

Deposition — With the maximum interparticle force and total particle charge it is possible to calculate the voltage gradient that would produce a force on the particle equal to the maximum interparticle repulsive force. This works out to voltage gradients of 470 V/cm and 250 V/cm for the 6 and 18 μMolar cases respectively. Given the uncertainty in the measurement and calculation of the interparticle potential, this result is in good agreement with the observed voltage gradient necessary for deposition of 300 V/cm. Based on the above analysis it is reasonable to believe that deposition of the particles in this case occurs primarily by electrostatic force on individual particles.

5.2.4 Additional Issues in Ag/Pd Deposition

The deposition of Ag/Pd illustrates two effects that can occur during deposition. The first, ramified growth, is unique to the deposition of metal particles. The second, gravitational convection, is an effect that will occur in any deposition system where the particles are denser than the solvent, except when the deposition is performed straight down.

Ramified Growth — As soon as conductive particles contact the deposition electrode, because of electronic conduction they will take on the electric potential of the deposition electrode. Deposited particles that extend from the deposition electrode will concentrate the electric field at their tip. This will attract other particles to deposit on the highest point, leading the growth of dendrites. This behavior is illustrated diagrammatically in Fig. 5.4.

The actual effect of this growth on a deposition is shown in Fig. 5.5(a) below. Here there are two electroded areas at the top and bottom of the picture. Across the center of the picture is a 25 μm horizontal line of bare glass. The edges of the electroded areas are straight, sharply defined lines. These electroded areas are covered by a deposition of Ag/Pd powder 3 to 4 particle diameters deep. It can be seen that lateral growth of the deposited metal particles has both narrowed the line as well as created a very irregular edge.

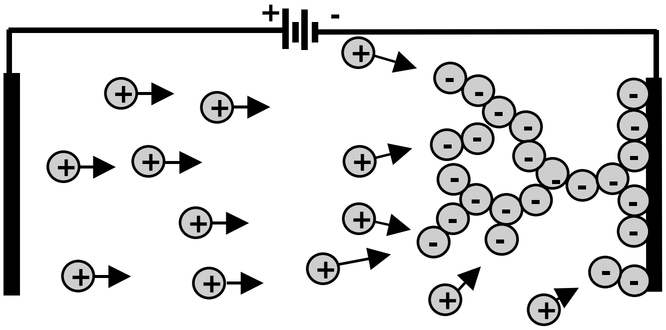

Fig. 5.4 In electrostatic deposition of conductive particles the particles will assume the charge of the deposition electrode.

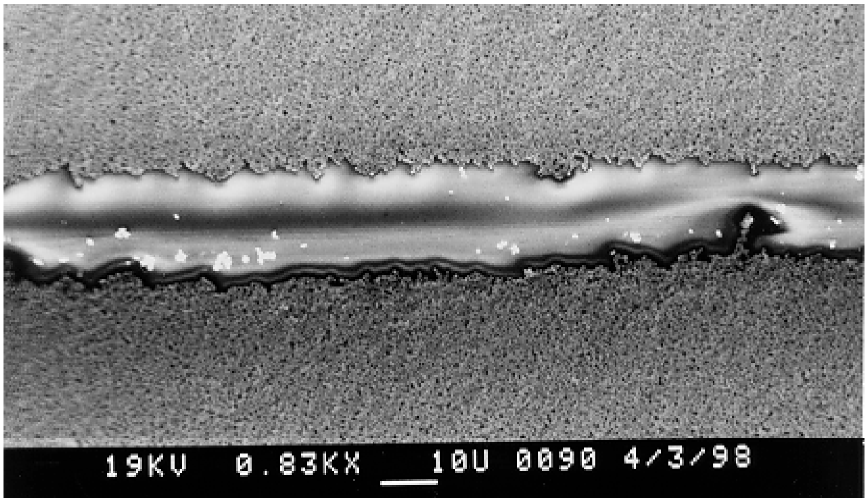

Fig. 5.5(a) Example of the lateral growth of a deposition over an non-electroded line.

At the edge of an electroded area the growth away from the electrode edge will be much more pronounced, as shown in Fig. 5.5(b).

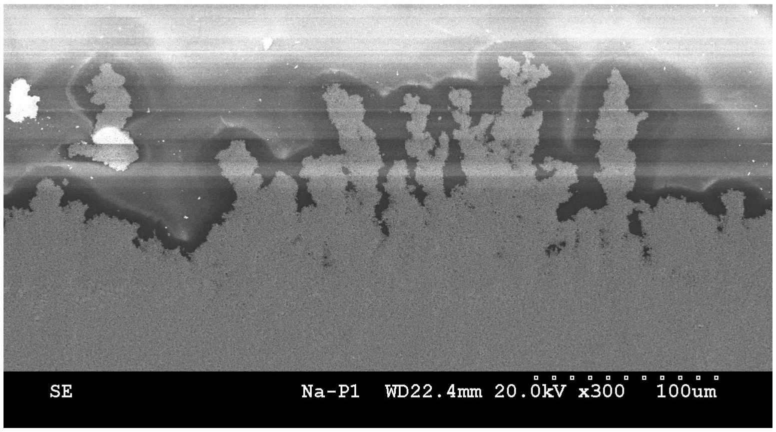

Fig. 5.5(b) Example of the lateral growth of a deposition at the edge of an electroded area.

If deposition is accompanied by EHD convection around the electrode it can drive the particles to deposit in a pattern dictated by the EHD flow. In Fig. 5.5(c) parallel vortices flowing out of the main deposition area cause the extension parallel fingers of deposition instead of fractal trees.

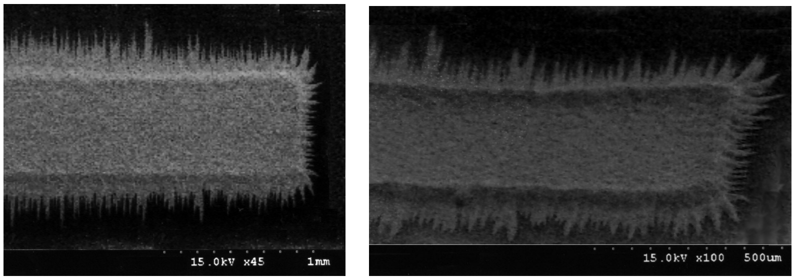

Fig. 5.5(c) Example of the lateral growth of a deposition at the edge of an electroded area influenced by EHD convection.

Gravitational Convection — Another significant complicating effect that commonly occurs in EPD is gravitational convection. As particles are driven away from the counter electrode, the pure fluid layer that forms there will have a lower average density than the fluid containing particles. This fluid will then rise to the top of the cell. This gravitational convection will often dictate the flow direction of EHD convection, with EHD forces adding to the speed of the gravitational convection. In vertical deposition electrode cells this can often lead to a deposition which thickens toward the bottom of the cell. A crossection of this type of convection occurring in a suspension of Ag/Pd is shown in Fig. 5.6. The black areas are dense suspension, light areas are solvent depleted of particles.

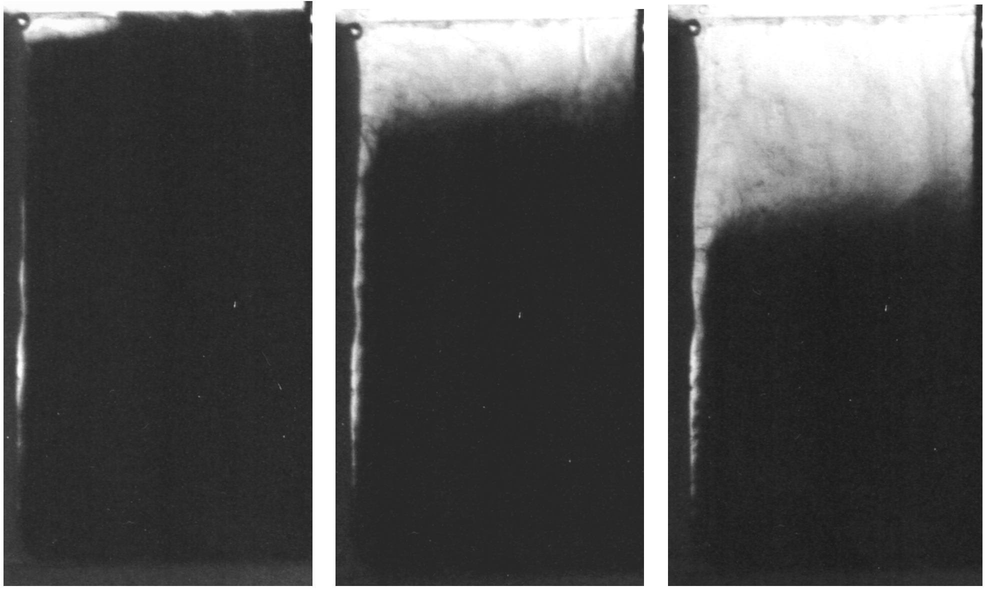

10 sec. **30 sec.** **60 sec.**

Fig. 5.6 Gravitational convection of Ag/Pd caused by electrophoresis. The particles are driven away from the vertical electrode on the left toward the electrode on the right. Fluid next to the electrode on the left is depleted of particles. With a much lower average density this fluid rises upward, eventually filling the top portion of the cell.

5.2.5 Uniform Coatings on a Rigid Substrate

A very common operation in electronic manufacturing is the formation of a uniform metallic coating. These are formed by sputtering, screen printing, electroplating and electroless plating. They are sometimes used as a continuous layer for a ground plane or electronic shielding. Very frequently these continuous layers are masked and etched to produce circuit patterns. Here the objective was to produce an electrode which would be stable and compatible as a bottom electrode for an EPD formed PZT layer to be sintered at 850°C. (**11**)

Demonstration — Shown in Fig. 5.7 below is a one micron layer of silver/palladium that was formed by EPD onto a standard alumina circuit substrate and sintering of the deposition. The substrate was prepared by sputtering of a 40 nm platinum coating to make the surface conductive. The electrode spacing was 2 cm, 500 V was applied for 45 seconds generating a current of 42 μA/cm^2. After rinsing the dried deposition weight was 1.0 mg/cm^2. The deposition was densified by heating to 900°C at 15°C/min and allowing to cool at a maximum 15°C/min. The resulting coating was uniform, adherent and examination by SEM revealed no through thickness pores greater than 1 μm.

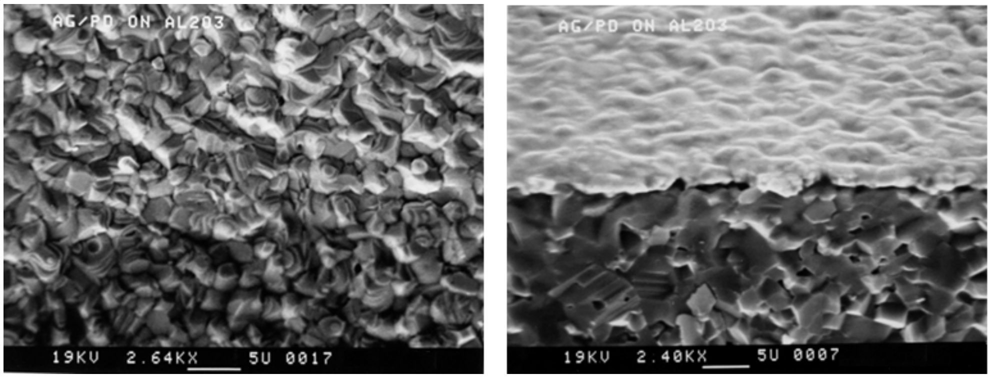

(a) (b)

Fig. 5.7 One micron thick Ag/Pd layer on an alumina circuit substrate, (a) top view, (b) oblique view of fracture edge, Ag/Pd on top, fracture surface of substrate below.

To create a film of this thickness by sputtering would take as much as an hour. To produce a one micron coating of a single metal such as copper by electrodeposition would take only a little longer than electrophoretic deposition and would not need a sintering step to densify the coating, however, forming a coating of an alloyed metal by electrodeposition is a much more difficult and involved process when it is possible at all. Screen printing can rapidly create a coating of an alloyed powder, but cannot produce a uniform continuous coating at this thickness on a rigid substrate. EPD is unique in being able to produce a controlled stoichiometry alloy layer rapidly and inexpensively in the one micron thickness range.

5.3 Use of EPD in Multilayer Fabrication

While EPD may have advantages for the production of continuous coatings in certain cases of electronics manufacturing, it is in multilayer electronic device fabrication where EPD has the potential to dramatically improve the state of the art.

The current standard technology for production of multilayer electronic devices consists of: 1) casting of a continuous dielectric particulate tape layer, 2) punching and filling of vias through the continuous tape to provide interconnection between layers, and 3) screen printing patterns of conductor, resistor, inductor and capacitor materials onto the continuous tape. These multicomponent tapes are then stacked, laminated under pressure to fuse the layers together, and sintered to form the final device.

EPD has the potential to reduce the scale of these multicomponent tapes by an order of magnitude over current technology both in thickness and lateral dimensions, improve the uniformity the final device, and remain cost competitive with current high volume production techniques. The demonstrations below cover the forming of continuous layers, forming of a continuous thickness multicomponent tape, creation of micron scale patterns, and a discussion of the forming of multicomponent tapes completely by EPD.

5.3.1 Forming Continuous Layers for Multilayer Devices

The simplest application of EPD is in the creation of uniform thickness tapes, such as are currently produced by doctor blade tape casting. To do this the entire tape carrier is coated with a conductive layer. A voltage is applied to the carrier in a deposition bath and a uniform layer of the particulate material is deposited. Binder can either be dissolved in the solvent for the EPD bath or can be introduced into the tape in a second step.

The advantage of this process is the formation of a tape with more uniform particle packing than can be achieved by traditional tape casting. This in turn should lead to the ability to create uniform tapes that are significantly thinner than is currently possible. This is thinner both in absolute terms and in terms of the number of average particle diameters, i.e. thinner tapes could be created with the same size particles without loss of continuity.

Demonstration

The objective of this experiment was to determine the minimum thickness continuous electrode layer that could be formed using the 0.3μm Ag/Pd powder. Multilayer stacks were built up layer by layer with each layer handled on a polyester film carrier until it was laminated to the stack and the carrier peeled off.

The barium titanate layers were formed by screen printing onto a polyester carrier film. The screen printing ink was prepared using a standard tape casting binder (Ferro B73210) to allow for lamination of the films. The barium titanate powder used was Cabot BT-8 coated with 5 wt.% bismuth oxide to promote sintering in the 700°-800°C range. The BT-8 average particle size is 0.2μm with a generally smooth, equiaxed particle shape. A 2.54 cm square pattern was printed through a 10μm thick screen and was dried at 80°C yielding a 2 to 4μm thick tape layer.

The silver/palladium was deposited onto 2.54 cm square pieces of polyester film with a sputtered platinum layer to make the deposition side conductive. A deposition voltage of 200 V/cm was applied 5 seconds on, 5 seconds off, for a period of 90 seconds (45 seconds on). No binder was added to the silver palladium layers prior to lamination.

Lamination was performed in a heated, uniaxial lamination press at 40 MPa and 70°C. The silver/palladium deposition was placed face down onto a barium titanate layer and pressed. Under these conditions there was enough diffusion of binder from the barium titanate layer into the metal powder to bond it to the stack. The platinum sputtered polyester could be peeled off the stack leaving all of the silver-palladium powder laminated to the layer below. The polyester retained its shiny conductive surface and could be used again for another deposition. A barium titanate layer was then laminated on top of the metal layer and the process repeated.

The results of the first laminate produced are shown in Fig. 5.8 below. The green cross section Fig. 5.8(a) shows the Ag/Pd powder layer that when sintered yields one of the 1.2μm layers shown in Fig. 5.8(b). The polished cross section examined in the SEM was 5 mm wide. The picture in Fig. 5.8(b) is representative of the uniformity of the Ag/Pd layers over the entire width of the specimen. No pores or gaps were seen over the 5 mm examined.

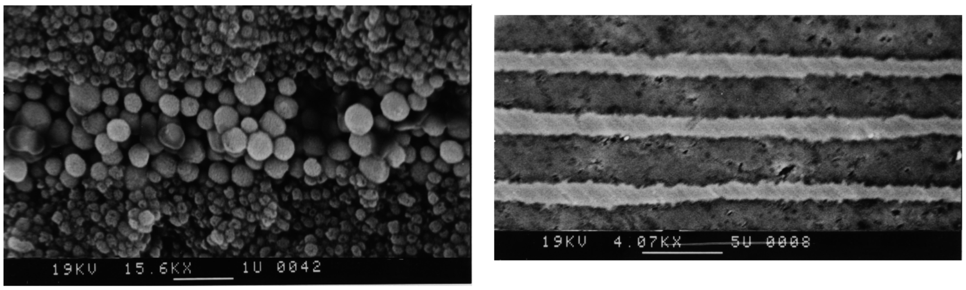

(a) **(b)**

Fig. 5.8 (a) Green cross section showing Ag/Pd powder layer (center) between barium titanate layers (top & bottom); (b) Polished cross section of sintered multilayer showing 1.2 μm thick Ag/Pd electrode layers (light color layers) between 2.5 μm layers of barium titanate.

The continuity and uniformity of these 1.2 μm layers are representative of what would be required of a dielectric layer. An electrode layer can have a significant number of through thickness pores while still maintaining electrical continuity. Based on the multilayer above it appeared that the electrode thickness could be reduced by half without losing continuity. To test this a second multilayer was made using depositions of Ag/Pd powder one half the thickness used in the first example. The depositions were formed using 200 V/cm applied continuously for 15 seconds. The resulting multilayer is shown in Fig. 5.9 below.

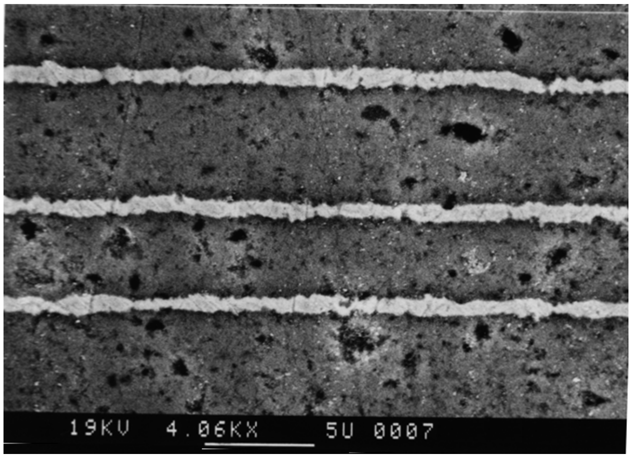

Fig. 5.9 Polished cross section of sintered multilayer showing 0.6 μm thick Ag/Pd electrode layers (light colored layers).

The silver/palladium layers formed averaged 0.6μm thick and were continuous across the width of the 5 mm sample prepared. Examination of the full 5 mm width of the polished cross section in the SEM showed very few pores that extended through the 0.6 μm layer.

What has been demonstrated here are the likely minimum thicknesses possible for two types of layer formed by EPD of equiaxed particles. For dielectric or membrane layers where there should be no through thickness pores or areas of significantly reduced thickness, the minimum thickness will be 4 - 5 times the average particle diameter. This corresponds to the four particle diameter thick layers in Fig. 5.9. For capacitor electrodes, ground planes or shielding layers it is only necessary to maintain connectivity in the plane of the electrode and significant through thickness porosity can be tolerated. Here the minimum thickness will be ≈ 2 times the average starting particle diameter. Prior experience in this lab at forming 50 nm thick layers by EPD of 10 nm diameter silver particles (**12**) strongly suggests that this thickness scaling based on average particle diameter will be valid throughout the nanometer region as well. By moving to the EPD of nanoparticles it should be possible to rapidly and inexpensively produce layer thicknesses that have previously only been possible using traditional thin film processes.

5.3.2 Tape Overcasting on EPD Patterns

Another application of EPD is to combine it with traditional doctor blade tape casting to produce a uniform thickness multicomponent particulate tape. By applying a voltage to a conductive pattern on the tape carrier, one type of particulate material can be deposited in that pattern onto the carrier. With multiple patterns more than one material could be deposited. This is followed by normal tape casting of the final material over the deposited components. The solvent containing the binder from the tape casting slip will impregnate the electrophoretically deposited components, incorporating them into the tape. By this means a uniform thickness tape can be produced that incorporates secondary materials for conductors, resistors, capacitors, etc.

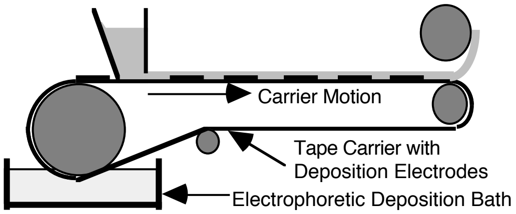

Fig. 5.10 Combining EPD on a tape carrier with tape casting can be used to create a uniform thickness, multicomponent particulate tape.

The advantage of this process is that it creates a uniform thickness multicomponent tape. In the traditional process a uniform thickness tape is cast and secondary components are screen printed onto the surface of this tape, making the thickness of the multicomponent tape uneven. When many of these tapes are stacked, low density areas can be left in the laminate. These cause stress concentrations which can serve will failure origins in sintering or use of the device.

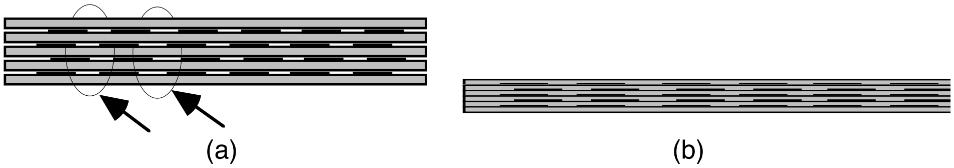

Fig. 5.11 (a) Uneven thickness leads to low density regions; (b) Laminate of even thickness tapes eliminates low density regions in green body

The key to this process is the thickness uniformity of the layers formed by EPD. This would allow a much thinner layer of material to be tape cast over the components already on the carrier than would be possible if the patterned components were screen printed onto the carrier.

Demonstration

There were two particular questions that the tape overcasting experiment was intended to answer. The first was whether a patterned deposition of metal powder, which contains no binder, would retain its pattern during the tape casting operation, or whether casting the tape over the deposition would wipe out the pattern. The second question was whether the binder from the tape casting slurry would penetrate into the metal powder deposition, incorporating it into the tape, and allowing the two component tape to be peeled cleanly from the glass carrier.

To test this concept, a glass plate was used as a tape casting substrate. An area of the plate was coated with a sputtered platinum electrode and 25μm lines were scribed into the electrode. Depositions of 1.0 to 2.5 μm were made onto the glass surface by continuous application of a 300 V/cm electric field for 30 to 90 seconds. Deposition thickness was determined by weight gain of the glass substrate and later confirmed by direct scanning electron microscopy (SEM) examination of the green tape cross section. A 75 μm thick barium titanate tape was cast over the deposition using a traveling slip hopper with doctor blade.

The results are shown in the pictures below, Fig. 5.12. Fig. 5.12(a) shows the generally rectangular Ag/Pd deposition area on the glass carrier with vertical line pattern at the top edge. Fig. 5.12(b) shows the cast tape as it is peeled off the carrier. The top half of the picture shows the bottom of the cast tape as it is peeled up. The bottom half of the picture is a reflection of the rolled up tape off the glass carrier. The gray is the metal powder deposition incorporated into the white barium titanate tape. The pattern of lines scribed in the deposition electrode is still clearly visible as white barium titanate lines between gray areas of the metal deposition.

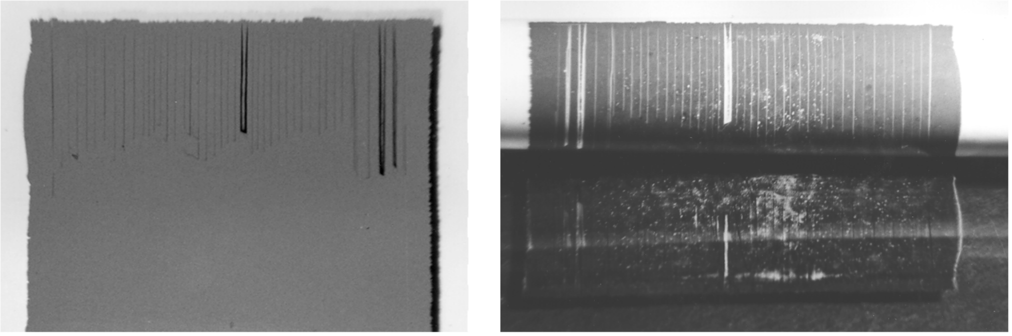

(a) (b)

Fig. 5.12 (a) 2.5μm thick patterned deposition of Ag/Pd powder on a glass tape casting substrate; a barium titanate slip was cast over this deposition and in (b) the peel up of this barium titanate cast tape is shown incorporating the patterned Ag/Pd deposition.

5.3.3 Deposition and Lamination of a Conductor Pattern

Patterned components can also be incorporated into a multilayer by direct lamination of a patterned deposition to the stack. A patterned deposition electrode is created on a carrier and a particulate material is deposited on this pattern. Then the carrier is then placed on the laminate stack, heated and pressed to incorporate the patterned deposition into the laminate. After lamination the carrier film with the conductive pattern can be peeled off and reused without needing to recreate the conductive pattern. The layers between the patterned layers formed by EPD can be tapes cast by standard methods. The deposition can either be infiltrated with binder before lamination or can be laminated dry allowing excess binder to flow from the layer below it, bonding the deposited material.

The advantage of using EPD in this process is the incorporation of secondary components into a laminate stack with better particle packing, lower thickness and finer detail sizes than is possible with other printing techniques.

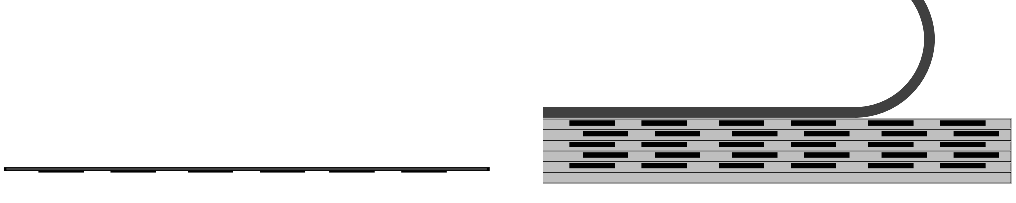

(a) (b)

Fig. 5.13 (a) Carrier with patterned deposition of material; (b) Carrier film is peeled off after lamination of the patterned deposition to the stack.

Demonstration

The first step for this demonstration was the preparation of a patterned deposition electrode on a polyester film. A resolution test pattern shadow mask was created by electron beam lithography at the Penn State Nanofabrication Facility. This resolution test pattern includes details from 50 μm down to 1 μm.

Polyester tape casting film was cleaned by wiping with optical quality tissue using alcohol and acetone to remove any coatings or contamination on the surface. The film was spin coated with a UV photopolymer mask and exposed through the shadow mask in contact mode. The unexposed photopolymer was rinsed off exposing a patterned area of bare polyester. The entire surface is then sputter coated with platinum. The photomask and overlying platinum were removed by sonication in alcohol. Well defined conductive lines down to 2 μm were achieved with relatively little effort.

A layer of Ag/Pd powder approximately 1 μm thick was deposited on the pattern by pulsing the voltage field 3 seconds on/ 3 seconds off for 90 seconds at 150 V/cm. The deposition was rinsed in a beaker of as-received acetic acid and allowed to dry. The carrier with the deposited powder was placed face down on to the shiny side of a stack of Dupont

951-A LTCC dielectric tape. This was laminated for 10 minutes at 200 MPa and 70°C. The polyester film carrier was peeled off the tape stack leaving the deposited Ag/Pd pattern as shown in Fig. 5.14

It is worth noting that the sputtered platinum showed remarkably good adhesion to the polyester film. No damage to the deposition electrode pattern was visible due to the initial sonication or in subsequent cleaning following deposition and lamination.

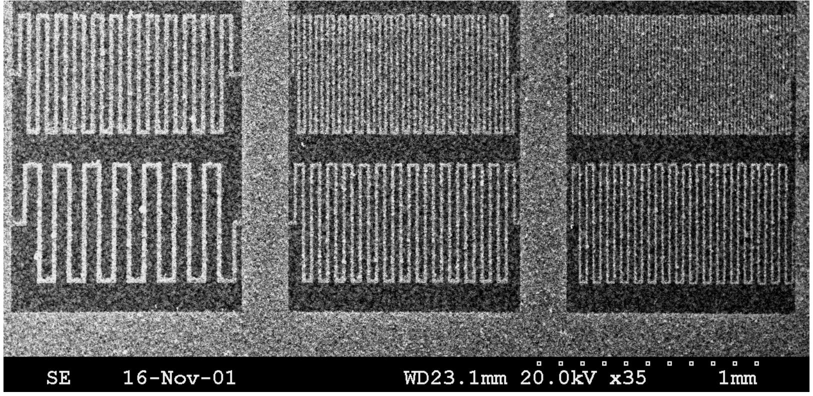

Fig. 5.14 DuPont 951-A LTCC tape with electrophoretically formed pattern laminated to the surface. Deposition electrode pattern line widths are 15, 10 & 5 μm. Powder deposition grows ≈ 2 μm beyond edge of deposition electrode edge. Graininess of image is due to porosity of the green tape.

The width of the lines on the deposition electrode pattern are 15, 10 and 5 μm. During deposition the powder deposit grows both laterally as well as in thickness. Here the powder deposit has grown approximately 2 μm beyond the edge of the deposition pattern. Because of this lateral growth, features on the deposition test pattern that had less than a 5 μm spacing between them were not distinguishable. The issues of the growth of the deposition beyond the deposition pattern and its implications for pattern resolution is a matter to be addressed in future publications. However, here we would like to note the primary obstacle to higher line resolution is the tape used for lamination. This tape is typical of a commercially available low loss dielectric tape designed for LTCC processing. Designed for secondary components added at screen printing resolution, the precast tape contains alumina particles ranging in size up to 5 μm. The low uniformity of the 5 μm line shown here is due in large part to the line being the same size as particles in the tape it is being laminated to. Taking advantage of the resolution which is possible using EPD-Lamination will require the development of a new generation of LTCC materials with particle sizes in the sub-micron or preferably nanometer scale range.

5.3.4 Multi-Component Deposition on a Multi-Electrode Substrate

The one aspect of the production of multilayer electronic devices that has not been demonstrated here is the formation of through thickness components. Currently these components are formed in an initially continuous tape by either mechanically punching or laser drilling holes into the tape. These holes are then backfilled with a second component. This process is usually restricted to tapes which are thick and strong enough to be handled off of a carrier. The smallest holes that are routinely formed and filled in this manner are 100 μm.

Multicomponent tapes with through thickness components can be formed by EPD using a carrier with a two part electrode pattern. This is illustrated in Fig. 5.15. The carrier would have a continuous electrode, a photopatterned polymer insulating layer, and a photopatterned top electrode. A voltage is applied to the top electrode in an EPD bath containing a dielectric powder. The deposition is rinsed and placed into a second EPD bath containing metal particles. There the second electrode is energized to produce a deposition with the same thickness as the dielectric material. This two component tape can now be laminated to a multilayer stack. The carrier with the deposition electrode pattern can be peeled off an re-used for another deposition. Because this layer is formed and handled on a carrier until lamination, the only minimum thickness limit is dictated by particle size as discussed in § 5.2.1 above. The minimum lateral dimension of the through thickness components is a subject for future experimentation, however, a lateral dimension two times the thickness of the layer is reasonable attainable.

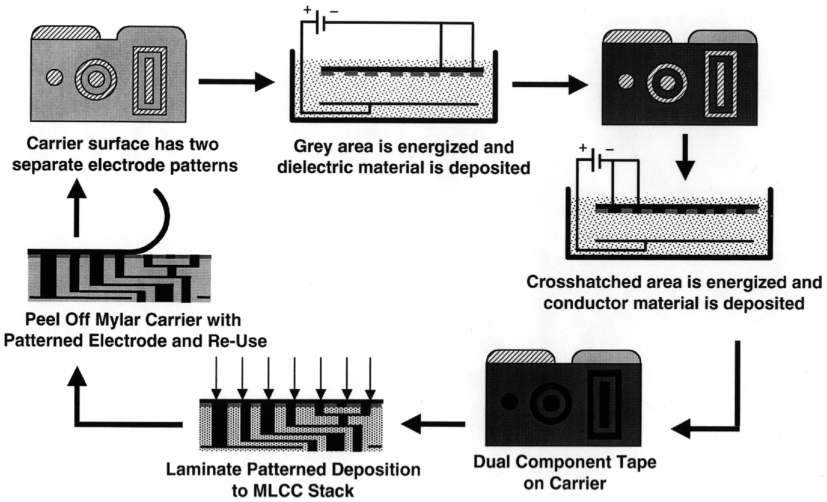

Fig. 5.15 Forming a multicomponent tape for lamination by successive depositions on a carrier with a two part deposition electrode pattern. The pattern illustrates the forming, from left to right, of a standard circular via, a shielded via, and a shielded in-plane conductor line.

In addition to a dramatic reduction in scale of these components, EPD can produce shapes which are not normally possible by punching and filling. The pattern in Fig. 5.15 shows how a coaxial via or a shielded in-plane conductor line could be formed by EPD of multiple components. The current best practice for lateral shielding in LTCC multilayers is the punching and filling of a discontinuous row of vias connected to the ground plane to form what is called a "via fence". (**13**) In contrast, EPD is able to form through thickness components as continuous lines, sharp corners, and, because the multicomponent tape is formed and handled on a carrier, cut out areas. There is no restriction that any single component be continuous to hold the tape together during processing.

5.3.5 Conclusions

This experiment was begun with an example electronic material, a 70/30 Silver Palladium Alloy 0.3 μm dia. powder, designed for co-sintering with a variety of electronic ceramics and in LTCC structures. This powder was dispersed in, and electrophoretically deposited from, a glacial acetic acid solvent. Estimation of the electrostatic stabilizing force indicate that the externally applied field used for EPD is of sufficient magnitude to overcome the interparticle repulsive force. This allows a mobile particle to come into contact with a stationary particle by electrostatic force alone. Thus for this case the growth of the deposition is attributed to the direct electrostatic force acting on each particle individually.

EPD of this Ag/Pd powder was used to demonstrate the formation of continuous electrode layers both sintered on a rigid substrate (constrained sintering) and within a multilayer laminate (free sintering). Based on observations of these layers the following minimum sintered thickness possible by EPD were inferred: for an electrode layer on a rigid substrate - 3 to 4 times the average diameter of the starting powder; for continuous dielectric or membrane layers in a co-fired multilayer - 4 times the average particle diameter; and for electrode layers in a multilayer requiring only in plane connectivity - 2 times the average particle diameter.

Patterned depositions were also produced on a carrier. The minimum line width demonstrated here is 30 times the average particle diameter. The likely minimum line width possible was not determined but will in part depend on matching the particle size of the material being patterned with that of the matrix material around it.

There are several ways to incorporate this patterned deposition into a multilayer device. One method is to cast a tape over the pattern by conventional methods to form a multicomponent tape that can be removed from the carrier. An alternative method is to laminate the pattern directly to a multilayer stack, removing the carrier after lamination. A multiple component tape can also be produced by multiple depositions on a carrier with two or more electrically isolated deposition patterns. If the resulting tape is continuous then it could be removed from the carrier for stacking or the depositions could be laminated to a multilayer while still on the carrier.

The key technological point here is that by depositing onto a photolithographically produced pattern then transferring the deposition to a multilayer structure, the pattern can be reused. A single photolithographic operation produces a deposition pattern which can be used to electrophoretically deposit multiple parts rapidly and inexpensively. Each of these parts can have details on a dimensional scale which was previously only possible by using lithographic process for each individual part. If a set of nano-scale powders are developed which can be dispersed, electrophoretically deposited and co-sintered, this process would allow the scale of circuitry in LTCC devices to drop by more than two orders of magnitude.

5.4 EPD of a Complex Lead Perovskite Particles

Three features of EPD cited in Ch. 1 as significant advantages over other film techniques are: better stoichiometry control than thin film vapor deposition techniques; better morphology control than sol-gel techniques; and creation of films in the 1 to 20 μm range which are difficult to produce by any of the traditional thin or thick film techniques. This section demonstrates each of these features of EPD.

To demonstrate stoichiometry control a complex lead perovskite was chosen. There are a number of important materials in the lead perovskite family, either solid solutions or compounds. $Pb(B_1,B_2)O_3$ compositions typically have high piezoelectric or electrostrictive activity, important examples of these are $Pb(Ti,Zr)O_3$ and $Pb(Zn_{0.33},Nb_{0.66})O_3$. There is an extensive literature on the compositional modifications of these compounds to optimize their function for specific sensor or actuator applications. Additional information on the application of these materials can be found in the recent reviews by Setter (**14**) and Whatmore (**15**). For the demonstration here a soft, niobium doped, morphotropic phase boundary $Pb(Ti,Zr)O_3$ was chosen. The demonstration of morphology control was not planned, but analysis of the dielectric behavior of the films suggest that grain size in the final film can be controlled by deposition conditions, independent of sintering. Finally, to demonstrate the ability to form films between 1 and 20 μm, films of 5.5, 8.5 and 13.5 μm are reported here.

This work is hardly complete. There are still many improvements in processing that can be made, and there are still significant questions to be answered about the behavior of these films. However, this is a compelling demonstration of the ability of EPD to produce high quality, complex oxide films in a very useful thickness range.

This section takes a narrative form in describing the iterative development of procedures to produce a PZT film with properties comparable to the bulk ceramic. To provide a reference point this section begins with a description of the PZT starting powder and a thorough characterization of its properties in bulk form. This provides a standard for judging the relative quality of the films produced. This is followed by a description of some of the solvent/additive combinations evaluated for dispersion of the PZT powder. The next step after dispersion is deposition, followed by sintering of the deposition to form a dense continuous film. Finally, electrical, electrothermal and electromechanical measurements are made on the film to compare film properties to the bulk.

5.4.1 PZT Powder - Bulk Properties

The PZT powder has a stoichiometry of $Pb(Zr_{0.52}Ti_{0.48})_{0.976}Nb_{0.024}O_3$. It was prepared by reactive calcination of the component powders followed by high energy milling to reduce particle size. High energy milling was conducted for 12 hours in a stirred ball mill with ≈ 3 mm dia. spherical zirconia milling media. The calcined powder was dispersed in de-ionized water with Tamol 963 (Rohm and Haas Co., Philadelphia, Pennsylvania), an ammonium salt of a carboxylated polyelectrolyte. pH was adjusted to 10 by the addition of ammonium hydroxide. After drying the dispersant was burned out by heating the powder to 500°C for 8 hours.

Particle size distribution as shown in Fig. 5.16 below was determined by light scattering (Mastersizer S, Malvern Instruments Inc.). Surface area as determined by single point BET adsorption is 3.2 m^2/g. A SEM micrograph of this powder is shown in Fig. 5.17.

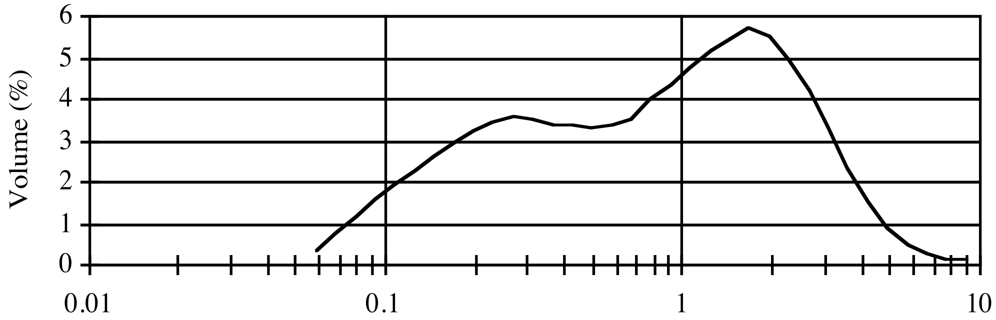

Fig 5.16 PZT particle size distribution , derivative volume percentage in microns diameter.

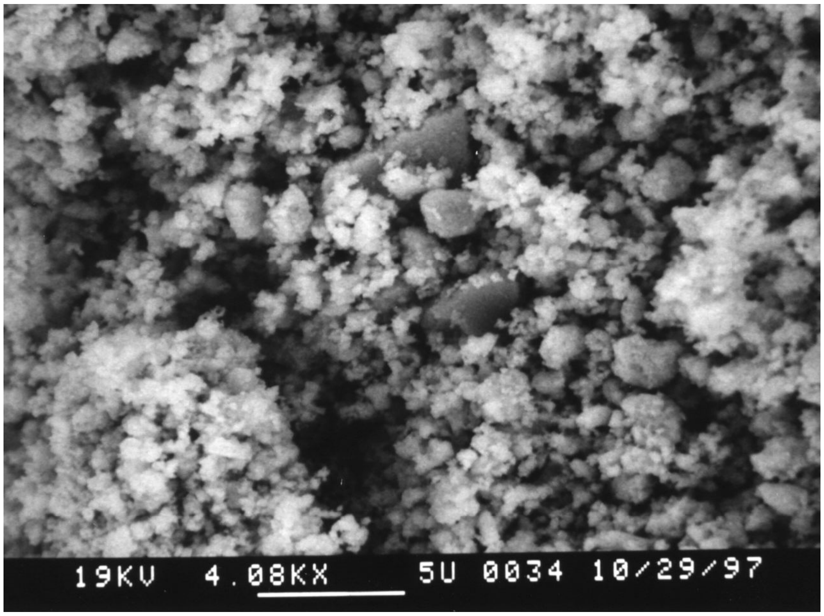

Fig 5.17 SEM photograph of attrition milled PZT powder.

Bulk samples of the sintered ceramic were prepared for property comparison. Six pellets were dry pressed and sintered in a sealed crucible with a lead source at 1,270°C for two hours. The pellets achieved an average final density of 96.2% with a standard deviation of 1.3% based on a theoretical density for PZT of 8.0 g/cc. Approximate dimensions of the samples were 1.4 mm thick x 11.0 mm diameter. The samples were sputter coated with gold top and bottom for electrical tests.

The average dielectric constant measured after sintering was 1,090 with a standard deviation of 70 and an average loss of 1.2%. The samples were poled at several conditions. Poling of three samples at 30 kV/cm and 80°C resulted in an average increase in dielectric constant of 44%. Raising the poling temperature on one sample to 120° C at the same voltage raised the dielectric constant by 58%.

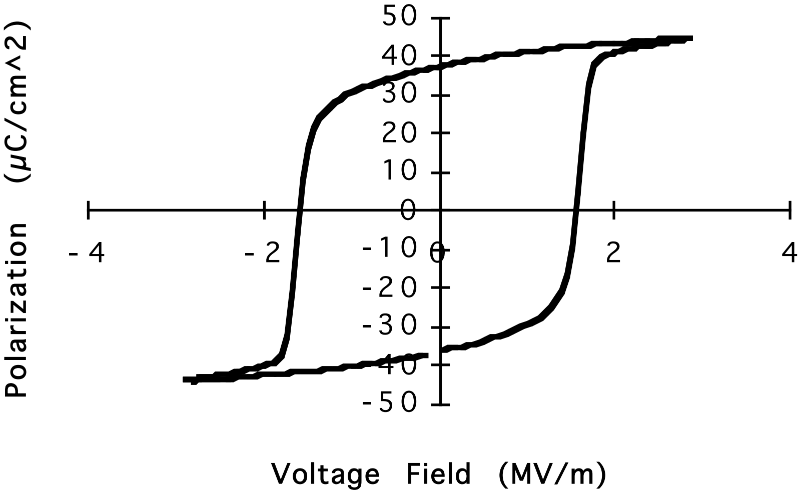

Fig 5.18 Polarization hysteresis on bulk sample, 5 second cycle. Remnant polarization 36.5 μC/cm^2; coercive field 15.9 kV/cm.

Polarization hysteresis was measured on three samples resulting in symmetric polarization hysteresis loops with an average remnant polarization of 34.1 μC/cm^2 and coercive field of 17.25 kV/cm. An example of these hysteresis loops is given in Fig. 5.18.

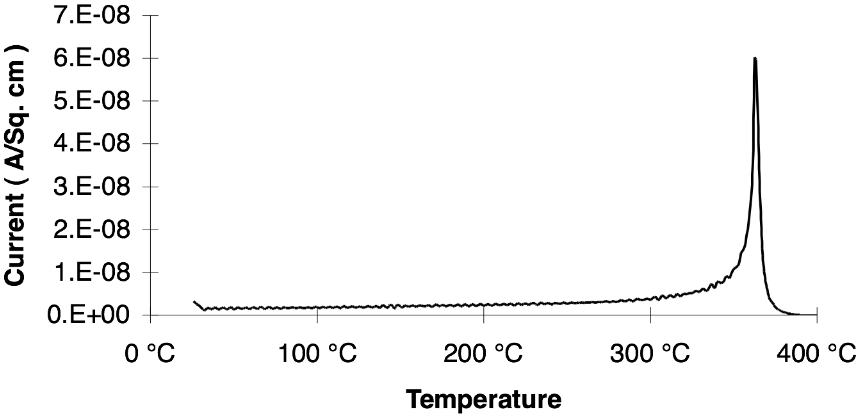

Fig. 5.19 Pyroelectric discharge current for bulk PZT.

A pyroelectric scan at a heating rate of 4°C/min. on one sample poled at 36 kV/cm and 120°C for 5 min. yielded a pyroelectric coefficient at room temperature of 45 nC/cm^2°K. The total discharge current was 41 μC/cm^2. Hysteresis was not measured on the sample used for this measurement, however, the discharge current is comparable to the average polarization measured on other samples. The maximum current occurred at 363°C and dropped below 1 nA/cm^2 at 377°C.

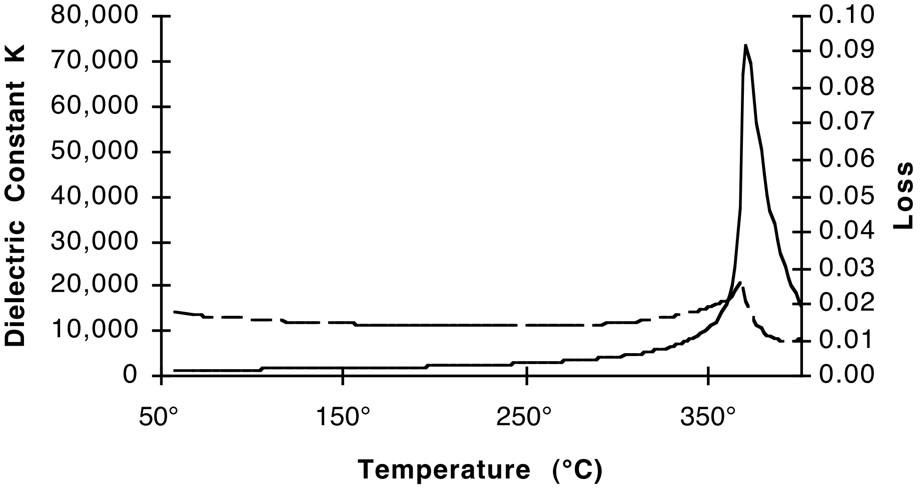

Fig. 5.20 Dielectric constant and loss as a function of temperature at 1 kHz with a 7 V/cm sine wave input.

Dielectric constant as a function of temperature showed a sharp peak at 370°C, with a maximum *K* approximately 50 times the room temperature value. This curve was measured on an unpolarized sample. To compare the relative breadth of peaks, the width in degrees was measured at a dielectric constant halfway between the room temperature and peak values. This yields a value of 19°C for this bulk sample.

5.4.2 Forming a Stable Suspension of PZT Powder

There was no systematic evaluation of dispersion systems for PZT, however, the experiments that were performed lead to a few observations. The first is the polarity of the surface charge that can be developed on the powder. Of the solvent-additive combinations tried, the PZT particles only developed a significant negative charge in water. In methanol, ethanol, iso-propanol, acetone and MEK the particles uniformly exhibited only a positive charge when charge was measured. This includes solvents with the basic additives such as ethanolamine or ammonium hydroxide.

Table 5.1 Solvent-additive combinations showing some dispersion effect on PZT powder.

Solvent	Additive	Dispersion Effect	Comments
Water	—	No	
	Ethanolamine	No	
	NH_4OH	No	
	Tamol 963	Yes	Ammonium salt of carboxylated polyelectrolyte (negatively charged adsorbing polyelectrolyte, electrosteric stabilization)
Ethanol	—	No	
	Emphos PS-21a	Yes	Phosphate ester of alcohol ethoxide (weak acid, electrostatic stabilizaton)
	Ethanolamine	No	Insufficient charge for electrostatic stabilization
	Iodine	Yes	Forms iodic acid, creates positively charged electrostatically stabilized suspension
	Lecithin	No	
	NH_4OH	No	Insufficient charge for electrostatic stabilization
	OLOA 1200	Yes	Polyisobutene succinimide (Straight chain hydrophobic polymer with negatively charged adsorbing end group, steric stabilization.)
	PEI	Yes	Polyethyleneimine (Amine groups at end of branches adsorb to negative surface sites, electrosteric stabilization)
	Tamol 963	Yes	
	Triethylamine	No	
Acetone	—	Yes	Positive surface charge, very low conductivity, electrostatic stabilization, difficult to reproduce
	I_2 in 2-Propanol	Yes	Forms iodic acid, creates positively charged electrostatically stabilized suspension
	Ethanolamine	No	
	NH_4OH	No	
2-Propanol	—	No	
	Iodine	No	
Xylene	OLOA 1200	Yes	

This matches the second observation regarding surfactants. Most of the surfactants that showed some improvement of dispersion of PZT were anionic, i.e. negatively charged, polymers. The negative groups on these polymers presumably adsorb to positive sites on the particles. The polymers then provide steric or electrosteric stabilization.

The exception to this is Polyethyleneimine (PEI). This is a highly branched polymer with amine groups at the end of each of the branches. It is possible that the amine groups on the polymer alter the solution chemistry enough that a negative surface charge is formed on the particles, allowing adsorption of the positively charged polymer. However, it is more likely that the amine groups displace another positive adsorbate at negative sites on the particle surface. No deposition attempts were made from polymerically stabilized suspensions, however, Ch. 2 suggests ways this might be attempted.

5.4.3 Deposition

Depositions were successfully accomplished from pure acetone, acetone with added iodine in 2-propanol, and pure acetic acid. Although the most uniform depositions came from the suspensions in acetone, it was easiest to repeatable produce depositions from glacial acetic acid, therefore this was the system that was most extensively studied and produced all of the films studied in section 5.3.4.

5.4.3.1 Acetone

Two depositions were produced from a suspension of PZT in pure acetone. 2.7 g of PZT powder was placed in a 200°C drying oven for one hour to drive off adsorbed water. This was directly quenched into 75.5 g of acetone containing 0.3 wt. % water. The powder was then dispersed by sonication. Deposition was carried out in a 200 ml pyrex beaker between two horizontal stainless steel disks spaced 2 cm apart and filling substantially all of the crossectional area of the beaker. Exposed plate area was 26.8 cm^2.

Deposition was conducted at a constant current of 0.1 mA or 3.7μA/cm^2. The negative pole of the current source was applied to the top plate. The particles in suspension were positively charged and were deposited vertically upward onto the top plate. The initial voltage when current was first applied was 39 V. This indicates a suspension conductivity of $\approx 0.2\ \mu$S/cm. A five minute deposition was accompanied by an accelerating non-linear voltage rise of 171 V. The thickness of the resulting deposition was not measured, however, visual estimation would put the thickness between 5 and 40 μm. The coating was very smooth, even, continuous and complete with no visible indications of convection.

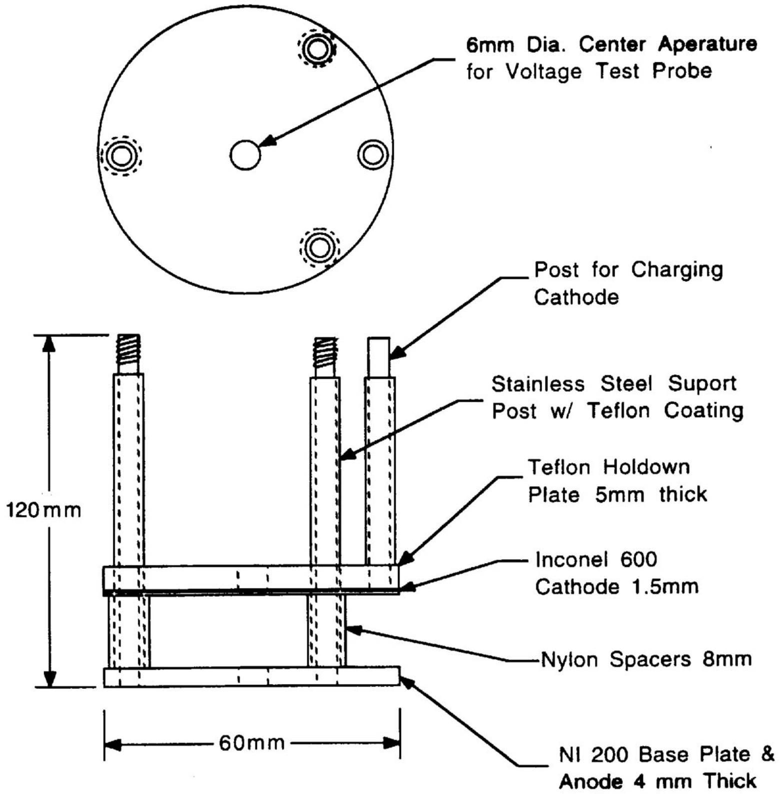

Fig. 5.21 Deposition test device.

Discussion —The powder develops a positive surface charge in pure acetone, although the charging mechanism is not clear. It is possibly due to acetone being very slightly acidic relative to water, thus generating a slight hydronium concentration in the solvent which preferentially adsorbs to the powder surface. Most of the powder sediments out immediately, however the suspension remains dense enough that the sedimentation is not visible. This would indicate that there is a positive electrostatic energy barrier to floccing which is insufficient for long term stability, but sufficient to retard floccing. Sedimentation will therefore initially be fairly rapid and become progressively slower as the volume density in the suspension decreases. In this case the suspension density is decreasing even as the deposition is progressing.

The large voltage rise at constant current indicates that the deposition is consolidated by the ion depletion mechanism in the deposited layer. This conclusion is further supported by the thickness uniformity of the deposition. Because of the low interparticle repulsion it is possible that the particles are initially deposited due to either the density increase or direct electrostatic force. However, there was no evidence of a low density surface layer, therefore it is likely that the ion depletion layer grows at the same rate as the overall deposition.

One advantage of this deposition is automatic size segregation of particles during deposition. Given that the suspension is only moderately stable, the surface potential of the particles must be between 25 mV, below which it is completely unstable, and 50 mV, above which it would have long term stability. This translates into a mobility somewhere between 0.1 and 0.2 μm·cm/V·s. Taking the midpoint and given an electric field in the bulk suspension of 20 V/cm, the electrophoretic velocity of the particles would be approximately 3 μm/s toward the cathode. The sedimentation rate of a 1 μm PZT particle is ≈ 3 μm/s. While an accurate force balance is slightly more complicated, it is clear that, in the absence of convection, the deposition will primarily composed of particles below 1 μm even though more than half of the particles by volume are above 1 μm diameter.

5.4.3.2 Acetone with Iodine in 2-Propanol

A slightly more stable suspension was produced by adding a small amount of a 2-propanol solution containing dissolved iodine. This suspension consisted of 2.3 g PZT, 81.5 g Acetone, and 0.92 g 2-propanol containing 0.5 wt. % dissolved I_2 and 0.06 wt. % water as determined by Fisher titration. The powder was dispersed by sonication while stirring for 2 minutes. This suspension was allowed to sit for ≈ 20 minutes before being poured into another beaker for deposition. The sediment remaining in the first beaker weighed 1.32 g indicating that 60% of the PZT powder either was not suspended or had sedimented out in the time it was sitting. The total solution depth in the first beaker was 3 cm.

Deposition was performed on a 2.54 x 2.54 cm alumina substrate with a sputtered platinum electrode on one side. It was suspended horizontally in the deposition beaker by a small clip in the center of one side with the electroded side down 1 cm above a stainless steel anode. The clip also served as electrical contact for the substrate. A constant current of 0.4 mA was applied for two minutes. The initial voltage was 16 V which rose at constantly decreasing rate to 23.6 V at the end of deposition. The total deposition weight was 14 mg. The deposition thickness was not directly measured, however a packing density of 60% in the deposition would give a thickness of 4.5 μm. As in the deposition from acetone alone, the coating was very smooth, even, continuous and complete with no visible indications of convection.

Discussion —Iodine dissolves rapidly in 2-propanol where it reacts to produce a concentration positive and negative ions. This is presumably through the creation of iodic acid, one possible mechanism for which is:

$$C_3H_7OH + H_2O \Leftrightarrow C_3H_7O^- + H_3O^+ \qquad \textit{Protolysis in Propanol/Water}$$

$$C_3H_7O^- + I_2 \Leftrightarrow C_3H_7OI + I^- \qquad \textit{Ionization of Iodine}$$

The concentration of iodine in the particulate suspension is 180 μMolar. If this was also the actual ionic concentration in the suspension, the Debye length would be only 6.4 nm, and it is unlikely that the suspension would show any level of stabilization regardless of surface potential. That this is not the actual ionic concentration is also supported by the low estimated conductivity of this suspension, 2 ± 1 μS/cm. Using the molar conductivity of iodic acid in methanol (**16**) as an estimate, this conductivity would translate into an ionic concentration of 10 μMolar. At this ionic concentration the calculated energy barrier to floccing would be 5 kT for two 0.5 μm diameter particles with a surface potential of 40 mV. The difference between the I_2 molar concentration and the ionic concentration is likely the result of both the incomplete ionization of the I_2 and adsorption of ions to the particle surfaces.

It is likely then that the addition of I_2 dissolved in 2-propanol increases the surface potential of the PZT particles in acetone by a slight preferential adsorption of the protonated species over the I^- ion. Given the voltage rise during deposition and the visual uniformity of the deposition, it is very likely that the deposition occurs by the ion depletion enhanced electrostatic mechanism. This would occur if the primary positive ion in solution is consumed at the cathode which is consistent with the ionization mechanism proposed above.

The difficulty in estimating the ionic concentration in this system is symptomatic of a larger problem in this system which is the instability of ketone-hydrohalous acid solutions. Tokuoka et. al (**17**) achieved very high ionic concentrations in acetone-I_2 solutions with 0.3 wt. % water. (However, they mention in a footnote that their solutions were not stable for more than one day.) Solutions prepared here, however, showed very low ionization in acetone with this concentration of water. Janz and Danyluk (**16**) reported a very low dissociation constant for hydrogen chloride in pure acetone, unstable conductivity readings, plus a number of possible polymerization or enolization reactions of the acetone catalyzed by the acid.

5.4.3.3 Suspension in Acetic Acid

The simplest suspension for the EPD of PZT was also the one with the best suspension properties; pure acetic acid. By adding PZT powder at a rate of 3 g per 100 ml glacial acetic acid, a suspension which is stabilized against floccing can be produced with no additives.

Solvent Chemistry — When the powder is added to the acetic acid, lead oxide on the surface of the powder will react to form lead acetate and water. The acid also reacts with zirconium to a lesser extent, leaving a titania rich surface. After thirty hours, some supernatant was removed for analysis by DC. plasma emission spectroscopy to determine the extent of dissolution/reaction of the particles. The following quantities were determined, expressed in mole percent of each element in the original powder: Pb 2.4%, Zr 0.6%, Ti 0.25%, Nb 0.9%. There was also some sodium remaining from the surfactant used during milling. The dissolved sodium in the supernatant was 0.01% of the total weight of the powder added.

Conductivity and Ionic Strength — The glacial acetic acid used had an initial conductivity of 0.04 μS/cm. This rose to 0.09 μS/cm after dispersion of the PZT powder. Without specific knowledge of the ionic species present or their mobilities, the same estimated molar conductivity as used in section 5.2.3 above, 6 μS/cm·mM, will be used. This gives an estimated ionic concentration of 15 μMolar which gives a Debye length of 23 nm.

Electrophoretic Mobility — The electrophoretic mobility of the particles was measured with the Delsa 440 laser Doppler velocimeter using the same process outlined in section 5.2.2 above, with a single potential of 30 V applied to the cell. The data points were fitted to a parabola, giving r^2 fitting parameters of 0.99 and higher. The calculated mobility at the stationary layers was 0.21 μm·cm/V·s. In a suspension not used for EPD, that mobility remained stable for 4 days.

Surface Potential and Surface Charge — Interpretation of this mobility in terms of surface potential is not straightforward. With a particle size distribution ranging from 60 nm to 6 μm dia. the boundary layer thickness parameter for this suspension, κa, ranges from 1.5 to 150. As shown in Fig. 2.19 this is in the center of the range where mobility changes as a function of relative boundary layer thickness. However, given the sedimentation rate of the PZT particles, the height of capillary in which the mobility is measured, 1.00 mm, and the time it takes to measure the mobilities through the height of the cell, ≈ 30 min., it possible to eliminate a large portion of the size range. In 30 minutes any particles larger than 0.35 μm dia. will have sedimented the entire 1.00 mm height of the measurement channel, while 0.25 μm particles will have sedimented by half the measurement channel height. The measurement procedure is to measure mobilities alternating between the top and bottom of the channel working toward the center, therefore 0.25 μm particles would be included in all measurements. Given that there was no significant difference between measurements between the upper and lower halves of the channel it is not unreasonable to estimate the average measured particle diameter as 0.20±0.05 μm. This gives a κa parameter of 9 ± 2. Since the surface potential is well above the ≈ 24 mV validity limit for the Henry formulation, the surface potential was estimated graphically from the results of O'Brien and White, Fig. 2.20 (**6**). This gives a surface potential of 54 mV with an uncertainty due to particle size of ±5%. This is within the error limits of the mobility measurement itself.

Inputting this potential into Eq. [5.4] gives an estimated surface charge density of 0.17 mC/m^2.

Electrostatic Stabilization — With an estimate for the surface potential and ionic strength of the solvent it is possible to make an estimate of the electrostatic stabilizing force. The L-VdW attraction and the electrostatic repulsion energies were calculated using the same estimation formulas as for silver/palladium in section 5.2.3 above. The result is shown in Fig. 5.22 below.

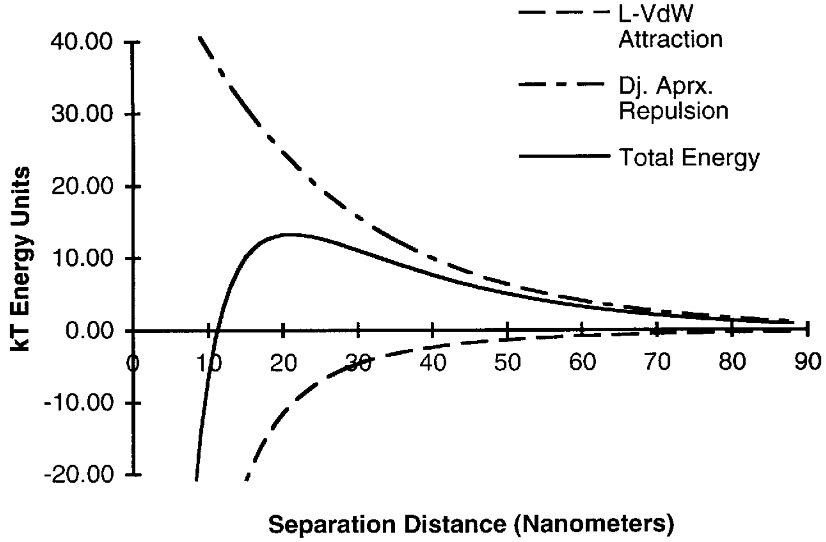

Fig. 5.22 Interaction potential for two 0.5 μm diameter PZT spheres in acetic acid; c = 15 μMolar; Ψ_0 = 54 mV.

The total repulsion energy between two surfaces will be a function of the areas of the surfaces that come into proximity. Therefore, the smaller the radius of the particle, the lower the total energy barrier to contact. Even though this stabilizing energy is quite high for larger particles, as can be seen in the picture in Fig. 5.16, these larger particles are much more angular than spherical. The repulsion at the low radius corners and edges will be much less than for a hypothetical spherical particle of the same size. Thus the stability of the suspension would be less that a straightforward combination of the particle size distribution and Fig. 5.23 would suggest.

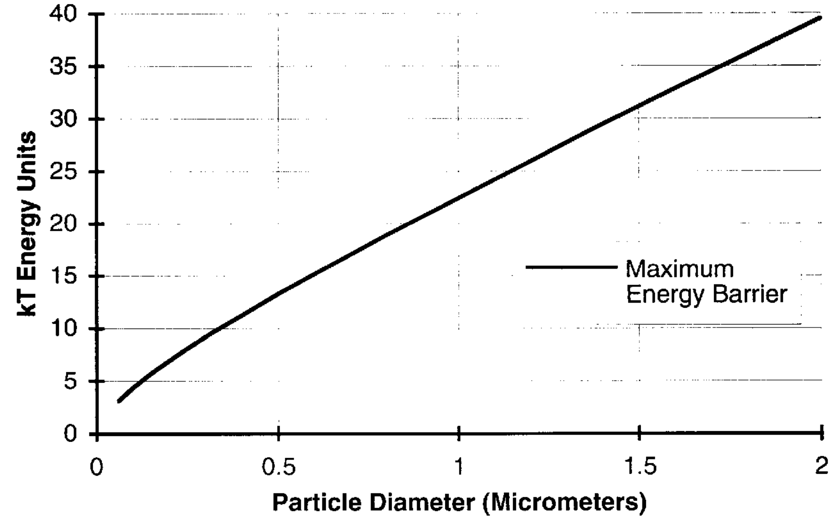

Fig. 5.23 Maximum repulsive interaction potential for two PZT spheres in acetic acid as a function of diameter; c = 15 μMolar; Ψ_0 = 54 mV.

Even if the particles are prevented from floccing sedimentation is a very significant factor in the behavior of these suspensions. The suspensions for EPD are prepared in a beaker with a fluid depth of 3 cm. As can be seen from the sedimentation velocities charted in Fig. 5.24, within five minutes of the end of sonication and stirring all particles above 5.5 μm dia. will have sedimented the full three centimeter depth of the suspension. Within 30 minutes the particles above 2 μm will have completely sedimented out as well. After 24 hours this would include all particles above 0.3 μm.

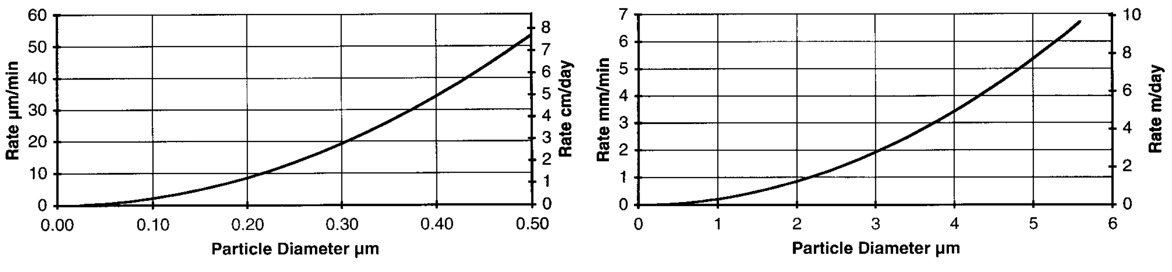

Fig. 5.24 Sedimentation speed for PZT particles in acetic acid at 25°C

Given that the particle size distribution extends down to 60 nm, if the particles were completely stabilized against floccing, after 24 hours particles below 0.3 μm should still be sedimenting out. Particles below 100 nm would show very little sign of sedimentation. As shown by Fig. 2.22, Brownian diffusion would keep a small but significant concentration 60 nm particles suspended indefinitely.

However, after 24 hours the PZT in the actual suspension will have completely settled out, leaving a crystal clear supernatant above a clearly defined sediment layer. This behavior lends considerable support to the measurements and calculations which are the basis of the size-stability chart in Fig. 5.23. Particles above 0.5 μm will have a large enough energy barrier to prevent floccing, but will settle out due to gravity. Particles below 0.3 μm which would stay in suspension longer have an energy barrier which is sufficient to slow, but not stop, floccing. These smaller particles will floc to each other and to larger particles forming masses that will settle out of suspension overnight leaving a completely clear supernatant.

5.4.3.4 Deposition from Acetic Acid

All of the films tested in § 5.4.4 below were deposited using a modified version of the deposition test device shown in Fig. 5.21. In this modification, shown in Fig. 5.25, the top Inconnel deposition disk is replaced with a 0.5 cm thick PTFE disk with a 5.20 cm^2 area square cut out in the center. A cylindrical PTFE holder block is fitted with spring mounted stainless steel wire hooks which both hold a 2.54 cm square alumina substrate to the face of the holder block and provide electrical contact to the face of the substrate. The holder block then mounts on top of the cut out disk so that the cut out masks the edges of the substrate. When a film is deposited the masked off area is not coated and provides an electrical contact point for the film's bottom electrode. The Ni 200 bottom disk then serves as the counter electrode. The cut out disk is held up by 1.5 cm spacers so that the total distance between electrodes is 2.0 cm. With these spacers the electric field gradient near the surface of the substrate is approximately 0.7 cm^{-1} times the applied voltage. For deposition the device is immersed in the particulate suspension in a 6 cm inside diameter Pyrex beaker.

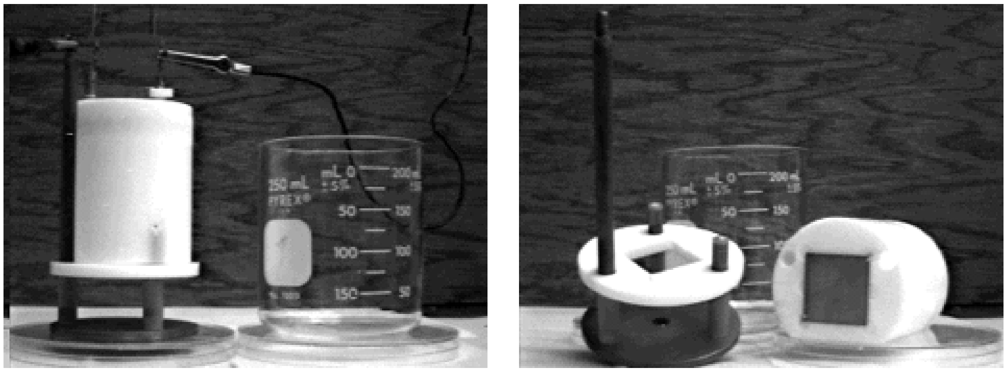

Fig. 5.25 Modified deposition device for deposition onto 2.54 mm square substrate. 5 mm thick PTFE disk masks the edges of the substrate with a 5.20 cm^2 square cut out area for deposition.

Depositions were performed at a constant voltage ranging form 100 to 500 V, which generated current densities from 1 to 100 μA/cm^2. Deposition times ranged from 45 seconds to 4 minutes, and depositions from 3 to 55 μm green thickness were produced. Most depositions were performed at either 250 or 300 V with a targeted final dense film thickness between 10 and 20 μm. During a typical deposition of 2 min. the current would rise by 1 to 2 % in the first 20 sec. followed by a decline over the deposition period also of 1 to 2 %. A subsequent deposition from the same system would then follow the same pattern, but would begin at a significantly higher current. Each successive deposition would then occur at a higher current until deposition was stopped or the suspension became too unstable to deposit. This conductivity rise occurred with both nickel and platinum counter electrodes, as well as during depositions of silver palladium from acetic acid using a gold anode.

Because of the significance of sedimentation, deposition should be started at the same elapsed time from the end of the sonication and stirring in order to insure reproducible results. To evaluate this reproducibility, a series of 16 depositions were made using the deposition device in Fig. 5.25. Before each deposition the beaker with the suspension and deposition device was placed in an ultrasonic bath for one minute while stirring. The beaker was removed from the ultrasonic bath, the holder block with a deposition substrate was placed on the deposition device and deposition was begun exactly 2 minutes after sonication was stopped. There were ten depositions of 90 sec. and six of 60 sec., all at 250 V. The deposition rate was linear with time with an average rate of 0.106 mg/cm^2•s and a standard deviation of 5.5%. The variation in the weight vs. time figure appeared to be random and did not show an up or down trend over the course of the experiment.

One important observation of these depositions was a large consolidation during drying. This was observable as a pronounced thickness change at the edge of the drying front as it moved across a deposition. Prior to drying the deposited powder showed clear pseudoplastic behavior. Using a point probe it is possible to manipulate the deposition like whipped cream or wet plaster and it will set in the rounded shape it is pushed or pulled into.

To evaluate this drying shrinkage, two depositions were made using platinum counter electrodes. Both depositions were made at 250 V for 5 minutes, after which they were removed from the holder block and rinsed by a single dipping in as-received acetic acid. One deposition was allowed to air dry while the other was placed onto a -10°C block of metal causing the acetic acid within the deposition to freeze in less than one half second.

The frozen deposition was freeze dried, impregnated with low viscosity epoxy, cut in crossection, polished and the thickness measured using an electron microscope. This procedure generated a density of only 25% for the freeze dried deposition vs. 60 % for air dried. This would suggest an almost minimum density flocced structure or very possibly some sort of ordered structure induced by EHD flows around the particles. Further work will have to be done to separate what specific structure may have existed in the deposition prior to freezing from structures which may be due to crystallization of the acetic acid.

Mobility measurements made one day later on suspensions that were used for deposition showed a mobility of only 0.14 μm•cm/V•s. This was accompanied by a doubling of the suspension conductivity compared to the initial suspension. Using the same procedures as above this generates a Debye length of 16 nm, and a surface potential of 35 mV. Using the Derjaguin approximation this gives a zero energy barrier to floccing.

This, however, does not always correspond with the observed behavior of the suspension. In some cases the suspension did become unstable after a certain number of depositions and further deposition became impossible. In many other cases, while floccing and sedimentation are slightly higher after 10 - 15 depositions, it is clearly not as rapid as in a completely unstabilized suspension. Furthermore, the fact that the deposition rate does not change, as shown in the reproducibility experiment above, implies that the electrophoretic mobility does not change significantly over the course of several depositions. If the electrophoretic mobility has not changed this would yield a surface potential of 50 mV, giving a energy barrier of 3 to 5 kT. This more closely matches the behavior of the suspension, observably floccing and sedimenting but over the course of 1 to 1 1/2 hours. This would need to be verified by mobility measurements made immediately after a series of depositions.

Conduction at the cathode appears to be by electrodeposition of lead ions and to a lesser extent titanium. Plasma spectroscopy measurements of the concentration of metals in solution in a suspension not used for deposition showed a concentration of lead of 2.0 milliMolar 90 minutes after preparation. Another measurement on the supernatant of a suspension which had been used for deposition showed a significantly lower concentration of dissolved lead. Unfortunately differences in sample preparation do not allow direct comparison of these concentrations. Additional evidence is provided by a substrate used for deposition. The alumina substrate with a polished platinum electrode was sintered at 1,250°C. This substrate was cathodically charged to deposit a coating of PZT. The deposition was later washed off so the substrate could be re-used. When the electroded substrate was heated to 950°C the electrode melted and the surface of the substrate turned blue. The melting of the platinum electrode can be accounted for by the formation of a low melting point lead-platinum alloy, and the blue color of the substrate can be accounted for by titanium doping of the alumina.

Discussion — Based on the observations above it is possible to begin to assemble a theory for the electrochemical and colloidal behavior of this system during deposition.

When PZT powder is placed in the acetic acid the lead oxide on the surface is rapidly converted to lead acetate in solution, along with a much lower concentration of zirconium and titanium acetate. The lead acetate is then very slightly ionized in solution to form a positive lead single acetate ion and a single negative acetate ion.

$$Pb(C_2H_3O_2)_2 \Leftrightarrow Pb(C_2H_3O_2)^+ + C_2H_3O_2^- \qquad \textit{Ionization of Lead Acetate}$$

The positive lead acetate ion is then preferentially adsorbed to the zirconate-titanate rich surface leaving a negative acetate ion in solution.

When a voltage is applied to the system, lead and titanium acetates will be reduced on the cathode. Because of the low current and the relatively large reservoir of un-ionized lead acetate in solution, ionic depletion at the cathode is not a significant factor in this case. This is supported by the constancy of the current during deposition.

At the anode nickel will be oxidized to form nickel acetate. If the nickel acetate has a higher ionization constant in solution this would account for the rise in ionic concentration, even though there is a 1 to 1 replacement of lead acetate by nickel acetate. As noted above this rise in conductivity also occurs with gold and platinum anodes. The creation of gold and platinum acetates are possible, but other possible anode reactions should be considered.

There are several mechanisms by which deposition can occur, however, it is useful first to rule out a couple of mechanisms. The first is simple densification. This mechanism requires a very low concentration in the bulk solution and a very low stabilizing force. This would be applicable as the conductivity and stability of the suspension goes down, however at this point deposition becomes more difficult and this would not account for deposition at the initial conditions where there is clearly a significant stabilizing force. The second is ionic depletion at the cathode. Although ions are consumed by electrodeposition at the cathode, if an ionic depletion layer were to form a drop in current would be expected as voltage was concentrated across the ionic depletion layer. Given the constancy of the current this mechanism can be discounted. Finally, there is increased ionic concentration. For this to occur there must be a mechanism for the production of ions at the cathode. However, this requires that there be a soluble cation for which the free energy of reduction is much larger than the free energy of the ion producing reaction. For this solution this would be the case where the hydrogen ion from an acetic acid molecule is reduced, producing a negatively charged acetate ion, in preference to the reduction of lead, titanium or zirconium ions from solution. This is a possibility, and if further work is done on this system it could be investigated. However, given the evidence of electodeposition of lead and titanium , it is unlikely.

This leaves direct electrostatic force. Given that the force distance profile and surface charge density is essentially the same as for Ag/Pd in section 5.2.3 above, the conclusion here is likewise that the direct electrostatic force is sufficient to overcome the interparticle repulsion. However, in this case the deposited particles will not assume the potential of the electrode. Deposited particles will remain positively charged relative to the solution and will retain a negatively charged boundary layer. This negatively charged boundary layer will flow away from the deposition electrode and will interact with the boundary layer of an approaching particle, which is also flowing away from the deposition electrode. The interaction of these EHD flows between the deposited and depositing particles is very likely to cause some structure to develop in the deposition layer. This structuring would account for the very low density of the deposition prior to drying.

5.4.4 Doping, Sintering & Properties

Having developed a procedure to electrophoretically deposit a thin, uniform, dense layer of PZT powder on a substrate, the next problem is to sinter this deposition to form a dense, continuous, polycrystalline PZT film on that substrate. The following section follows the heuristic as successive processing problems were identified and addressed to improve the quality of the films. While there is room for improvement in the final films produced here, the properties indicate that PZT films with good dielectric and piezoelectric properties can be produced from a particulate precursor down to a thickness of 6 μm. The successive steps taken here to improve film properties can serve to guide experiments to further develop these films.

The films were deposited and sintered on 25.4 x 25.4 mm alumina electronic circuit substrates (ADS 996, Coors Ceramics Co.). These are unpolished, 99.6 wt. % alumina substrates with the remaining 0.4 wt. % assumed to be a silicate based sintering aid.

5.4.4.1 Sputtered Pt Electrodes

For the first set of films the alumina substrates were made conductive on one side with a sputtered platinum coating ≈ 40 nm thick. The resistance across the substrate from corner to corner was 80 Ω measured using two point probes.

The first attempt at sintering an electrophoretically deposited coating was made by placing the coated substrate into an oven where is was heated to 1,270°C and held for two hours using the same heating and cooling profile as for the bulk samples in § 5.4.1. SEM examination showed a very low density, irregular coating. X-ray diffraction showed that all lead had been lost from the coating leaving only zirconate titanate.

The next series of sintering experiments were conducted in a small platinum metal box 2.6 x 3.0 x 0.5 cm. This box held one substrate and a small amount of lead source. The lead source is a 1:1 molar mixture of $PbCO_3$ and ZrO_2 powders. During sintering the powders will calcine to form $PbZrO_3$. The vapor pressure of PbO from the $PbZrO_3$ is higher than the equilibrium vapor pressure above PZT. PZT in the same environment should retain a stoichiometric lead ratio as lead is lost from the lead zirconate powder above 840°C. The platinum box enclosed the substrate and lead source but was not sealed.

Films were sintered at 100° intervals from 850°C to 1,250°C with a 20 minute hold at temperature. The films showed a progressive increase in grain size and density up to 1,150°. The estimated average grain sizes are 950°C - 0.3 μm; 1,050°C - 1 μm; 1,150°C - 2 μm. Had the progression continued to 1,250°C it may have fully densified, however, again at this temperature all lead was lost and only a very low density zirconate-titanate coating was left.

To address the problem of lead loss it was decided to try to lower the sintering temperatures of the films. Two sintering aids were tested to accomplish this, Li_2O and PbO. To dope the deposition with lithium, lithium carbonate was added to acetic acid where it reacted to form a 0.2 wt% lithium acetate solution. The dried deposition was then re-wetted with the lithium acetate-acetic acid solution, which was dried to leave behind lithium acetate which is burned to lithium oxide during the ramp up to sintering temperature. A weight of lithium acetate solution was added to the deposition sufficient to achieve a 4 mol. % concentration of lithium oxide. The dried weight of the lithium acetate was not detectable. The exact mechanism by which lithium works has not been determined, however samples sintered at 850°C and 950°C showed considerable grain growth and densification. The grain size and density at 850°C with lithium was intermediate between the size and structure of the undoped depositions sintered at 950°C and 1,050°C. The deposition with lithium sintered at 950°C showed a structure halfway between the undoped depositions sintered at 1,050°C and 1,150°C.

Lead oxide was added to depositions in a similar manner. Lead oxide was added to acetic acid where it reacts to form a lead acetate. A solution was prepared that was 10 wt. % based on lead oxide. A deposition was re-wetted with the lead acetate solution using a pipette. Sufficient solution was added so that after oxidation the lead oxide would be 44 vol. % of the deposited PZT. The excess lead oxide melts at 886°C, provides a transient liquid phase during sintering, and replaces the lead lost to dissolution in the EPD suspension. Since PZT does not form any excess lead oxide phases, PZT and lead oxide should co-exist as separate phases. Then, because of its volatility, the majority of the excess lead oxide evaporates during sintering, leaving stoichiometric or near stoichiometric PZT. This deposition was sintered for 20 min. at 950°C with a 45 minute rise time. This sample showed greater densification and less grain growth than the sample doped with only lithium.

The next step was to combine both lithium and lead oxide. Once again a deposition was re-wetted with lithium acetate to yield a 4 mol. % concentration of lithium oxide. Lead acetate was added to give a 66 vol. % ratio of lead oxide to PZT. The objective was to completely fill the pore structure of the 60 % dense PZT deposition, thereby taking advantage of capillary tension to assist in densifying the deposition as the lead oxide evaporated. This film was sintered at 900°C for two hours with a 45 minute rise time. A fracture crossection of the resulting film is shown in Fig. 5.26. SEM examination of this crossection showed porosity only at the top and bottom surfaces of the film. The top surface showed a grain size of ≈ 0.5 μm. Grain size in the bulk of the film was not measured.

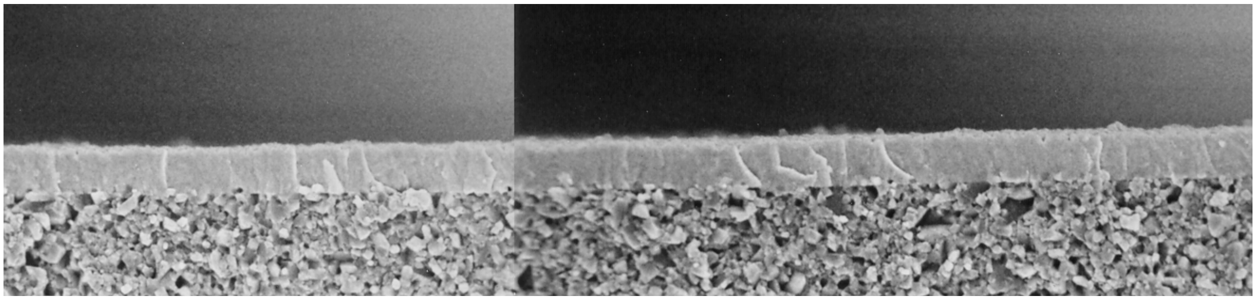

Fig. 5.26 Fracture surface crossection showing a 6 μm PZT film deposited on a dense alumina substrate with a sputtered platinum electrode (not visible) and sintered to full density at 900°C

As shown in Fig. 5.27, the X-Ray diffraction pattern for the film indicates that the film is phase pure PZT with no evidence of remaining crystalline lead oxide or of reaction with the substrate.

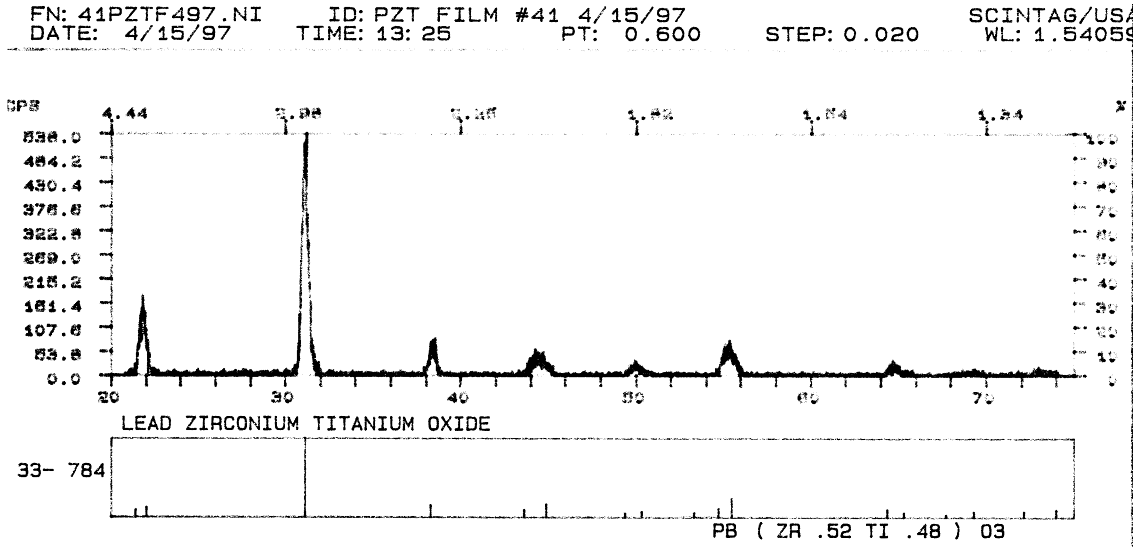

Fig. 5.27 X-ray diffraction pattern shows only PZT phase formed after densification

The weight loss of the substrate and film was equal to 75% of the excess lead oxide added to the film. The balance of the lead oxide appears to have been absorbed by the alumina substrate. There was a distinct yellow band in the alumina extending ≈ 0.3 mm below the PZT coating, as well as yellow staining around the edges of the substrate.

The sintering results for this film were very good, and the density achieved is better that any film produced subsequently. The results of these subsequent experiments strongly suggest that, even though the substrate contains only 0.4 wt. % silicate sintering flux, this flux diffused into the deposition and contributed significantly to sintering.

Unfortunately, during the sintering the thin sputtered platinum electrode de-wetted the interface, remaining only as small spherical inclusions scattered along the PZT-alumina interface. Without a bottom electrode electrical measurements of this film were not possible. The loss of the electrode as a barrier layer also is what allows the substrate's sintering flux to diffuse into the deposited layer.

5.4.4.2 Ag/Pd Screen Print Electrodes

To provide a stable electrode which would remain continuous and planar it was decided that a much thicker metal layer than is practical to produce by sputtering would be necessary. To do this the next set of substrates was electroded by screen printing of a 6/1 silver palladium paste. To minimize the through thickness porosity in the electrode layer, three layers of ink were screen printed and sintered. The surface was then polished to a mirror finish. The substrates were annealed at 950°C for 20 minutes to stabilize the electrode surface. The resulting electrodes were ~ 10 μm thick.

The platinum box used for enclosing single substrates during sintering was replaced by a covered zirconia crucible. Three substrates were placed flat, side by side on the flat bottom of the crucible with ≈ 1 gm of lead source in a zirconia boat. This was covered with a dish shaped lid having a volume of 94 cm^3. The edges were sealed with refractory cement which was porous enough to allow gas pressure equalization but prevents convective gas motion and slows gas diffusion in and out of the crucible.

It was found that the amount of lead used for sintering the high density film shown in Fig. 5.26 above was excessive in the presence of a continuous electrode layer. Sets of substrates were sintered with differing levels of added lead acetate. The level of lithium was kept targeted at 4 mol. % with actual levels varying between 2.5 and 4.5 % due to experimental error. The substrates were sintered at 900°C for two hours with a heating and cooling rate of 20°C/min.

The best results were achieved with the addition of lead such that the resulting lead oxide is between 25 and 34 vol. % of the deposited PZT. With less lead oxide the coating did not densify and remained a whitish color. Excess lead oxide causes several types of cracking, exaggerated grain growth and blistering of the electrode.

Re-wetting of the depositions with the lead and lithium acetate solutions was done by dripping the solution from a syringe. Drops frequently had to be placed at several points around the deposition the insure uniform wetting. Frequently, where the drop was added, the solution would wet the interface between the deposition and substrate much faster than the deposition. This would cause many small flakes of the deposition to come off the substrate where the drop was added. During drying the lead acetate did not end up distributed evenly through the deposition. The final areas of the deposition to dry ended up with significantly more lead acetate than the rest of the deposition. This was visible both on the dried deposition and as color and morphology changes over the surface of the substrate. Uniform, dense coatings had a dark brown color. A final sintering experiment did not show any sintering difference between a two hour and a half hour hold at 900°C.

Films that appeared continuous by visual inspection were electroded by masking with adhesive tape and sputtering 2.15 mm diameter gold circular spots on the surface. The resistance between the top and bottom electrodes was measured using steel tipped point probes. Spots with a resistance less than 40 MW were classified as bad. The electrical properties of film with the largest number of good spots are described below.

Film Preparation — The film which is described here, index #81, was deposited at 250 volts applied for 91 seconds with a nickel anode. This converts to an approximate voltage gradient near the deposition substrate surface of 175 V/cm. The deposition suspension was stirred in an ultrasonic bath for one minute and allowed to sit for exactly two minutes prior to the beginning of deposition. This resulted in the deposition of 9.4 mg/cm^2 of PZT. The film was re-wetted with lithium and lead acetate solutions sufficient to yield a 2.5 mol. % lithium concentration and lead oxide 20 vol. % of the deposited PZT. The film was sintered at 900°C for 30 minutes with a 20°C/min. heating and cooling rate. The resulting film had a dark brown area in the center surrounded by a lighter brown halo fading to dark brown again at the edges.

Film Properties — Twenty 2.15 mm diameter gold spots were sputtered onto the top surface of the film in a grid pattern. Of these spots, 13 were good, showing a resistance of more than 40 MΩ. Electronic measurements of these thirteen spots were used to generate the average property values reported in Table 5.2. To allow the direct comparison and correlation of quantities, one particular electroded area, Spot #7, was chosen for which a full set of measurements are reported.

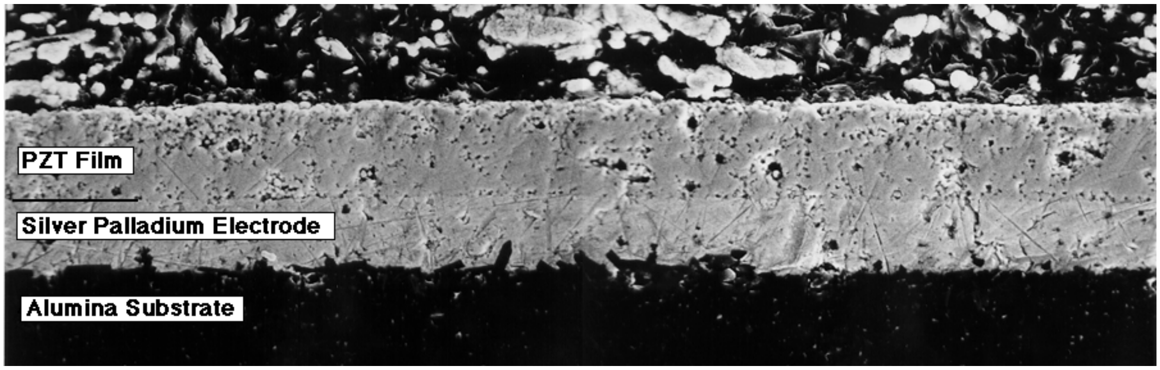

Fig. 5.28 Cut and polished crossection of PZT film. The layers from the top are: conductive silver epoxy; 13.5 μm PZT film; 10 μm Ag/Pd electrode; and alumina substrate.

A polished crossection of the film is shown in Fig. 5.28. This crossection was made through electroded spot #7. The average thickness measured in this crossection is 13.5 μm. Based on the deposition weight and film area, if the film were uniform and fully dense, the thickness would be 11.7 μm. Given that the apparent density at this point is well above 90%, it is likely that this area is slightly thicker than other areas of the film, and thickness variation will contribute to the variation in capacitance and coercive voltages. All calculated values below, however, were based on the directly measured thickness of 13.5 μm.

Capacitance was measured on an HP 4275A Multifrequency LCR Meter at 100 Hz and 1 Volt. This gives an electric field in the sample of 740 V/cm. This gave an average dielectric constant of 854 with a standard deviation of 8 % and an average loss of 0.049. Two spots which showed a loss of 0.12 and 0.15 were not included in this average. Spot #7 had a dielectric constant of 912 and loss of 0.045. Poling of spot #7 at 60 V (44.4 kV/cm) and 120°C for ten minutes produced an increase in dielectric constant of only 5 % accompanied by an increase in loss of 0.05.

The charge/voltage hysteresis was measured for all 13 electroded spots using a 20 Hz sine wave input with a maximum voltage of 130 Volts, giving a maximum field of 95 kV/cm. Average polarization was 16.5 $\mu C/cm^2$ with an average coercive field of 18.7 kV/cm. Many of the hysteresis loops were not symmetric. The average positive polarization was slightly lower than the negative polarization, 16.1 vs. 17.1 $\mu C/cm^2$, however the standard deviation of the positive polarization was 30% vs. 15% for the negative polarization. The hysteresis loop for spot #7 is shown in Fig. 5.29 below. The average remnant polarization is 23.4 $\mu C/cm^2$ with an average coercive field of 17.0 kV/cm. The positive polarization was measured at 27.5 $\mu C/cm^2$ with a negative coercive field of 21.5 kV/cm.

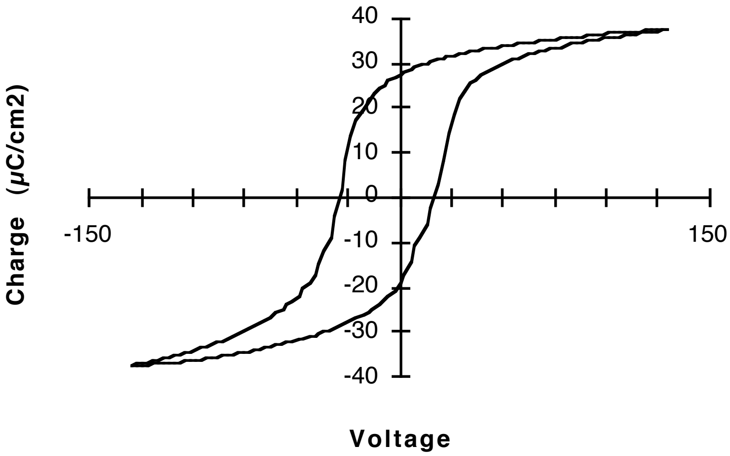

Fig. 5.29 Charge/voltage hysteresis loop for electrode spot #7, film #81.

The d_{33} coefficient was measured in a special test rig designed and built at Penn State (**19**). Spot #7 was positively polarized by the application of 150 V for 5 min. at room temperature. A wire was attached to the spot with silver filled conductive epoxy. In the test rig gas pressure is applied to both sides of the film substrate. The symmetric uniaxial loading is intended to prevent bending modes being induced during testing. The edges of the substrate project out of the pressure chamber between rubber O-rings. Thus the edges of the of the substrate are not exposed to the gas pressure. This means that the pressure on the substrate will be purely uniaxial, orthogonal compression of the substrate and film. The current used for calculating the piezoelectric coefficient was the average of the current in and out of the electrode when pressure is applied and released.

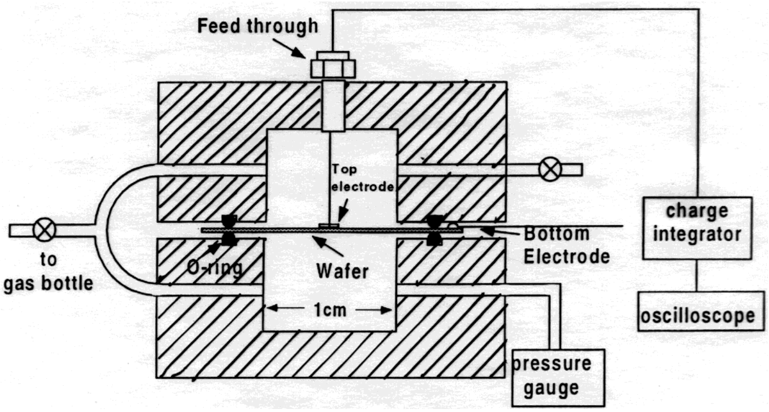

Fig. 5.30 Diagram of pressure cell for testing film d_{33} coefficient.

Applications of pressures of 0.5, 0.75 and 1.0 MPa gave, respectively, d_{33} values of 155, 151 and 137 pC/N. Because the highest pressure gave both the highest signal and the closest match between positive and negative current (10% difference), it is likely the most accurate measurement therefore an approximate value of $d_{33} \approx 140$ for this film was entered into Table 5.2.

Dielectric constant as a function of temperature was measured on a second film prepared at the same time and in the exact same manner as the above, but which was sintered for two hours at 900°C rather than 30 minutes. The estimated thickness of this film based on deposition weight is 14.2 μm. The dielectric peak is much lower than for the bulk sample, only 11 times the room temperature value and occurs at a temperature of 375°C. The peak is also much broader with a temperature span of 122°C at a level halfway between the room temperature and peak value.

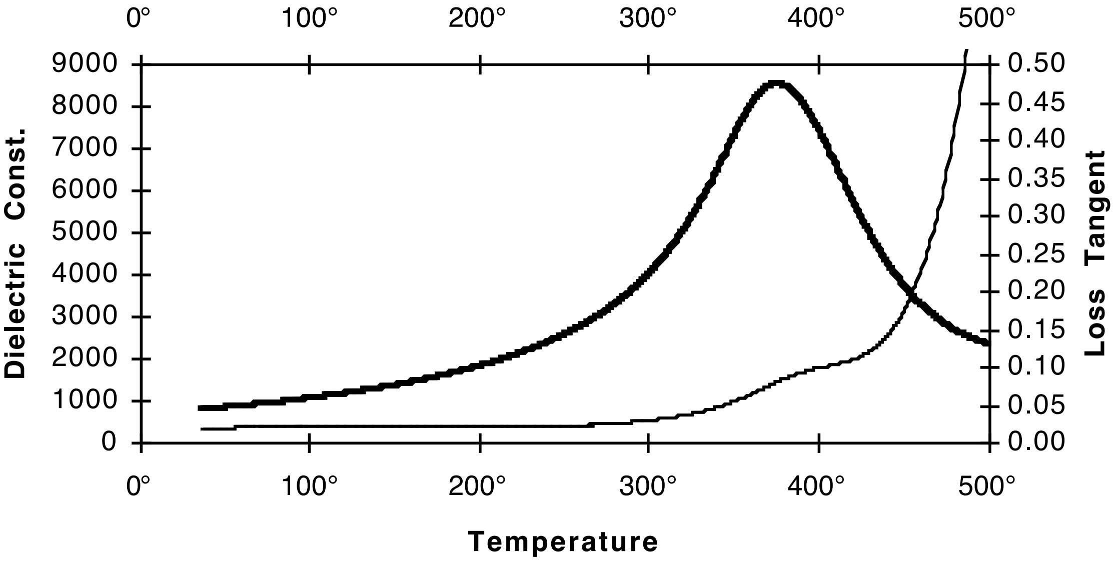

Fig. 5.31 Dielectric constant and loss as a function of temperature at 1 kHz with a 7 V/cm sine wave input.

Pyroelectric current was measured on a third sample which again was deposited at the same time as the first sample and was sintered together with the first sample. This sample had 10% more added lead and 30% more added lithium. Thickness calculated based on deposition weight is 15.0 μm. The first heating run showed a very large positive current, well beyond what could be accounted for by any dielectric polarization. At 335°C the current became negative and increased to -6x10^{-9} A at 400°C. The sample was reheated to 600° in between runs to sinter on a new Ag/Pd electrode contact. During this sintering the gold sputtered electrodes changed from a gold to silver color. It was then positively poled at 120 V for 5 min. at 120°C. The second pyroelectric current measurement did not show the same anomalous positive current but the negative current was even larger, reaching -10x10^{-9} A at 400°. For the final run the film was poled at -150 V for five min., followed by another poling at -120 V for five min. at 120°C.

Discussion — The uneven color of the sintered film likely corresponds to areas of different density in the film, lighter colored areas having lower density. This variation can be traced back to the uneven distribution of the sintering additives when the solution which the deposition is re-wetted dries.

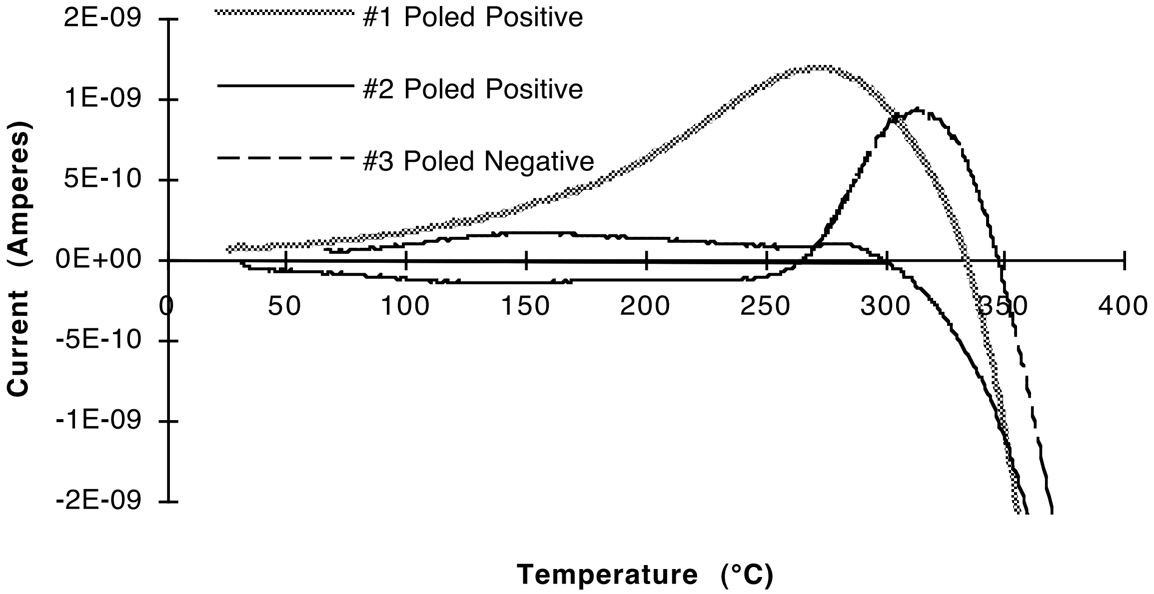

Fig. 5.32 Pyroelectric currents. Heating rate 4°C/min.

The room temperature dielectric and piezoelectric properties of this film compare fairly well the bulk samples. The bulk samples prepared by pressing contain the full range of particle sizes from the starting powder. That combined with the 1,270°C sintering temperature means that the grain size of the bulk sample would be 2 - 3 μm. For the film deposited by EPD the large particles will sediment out and will not be incorporated into the film. This combined with the lower sintering temperature of the film means that the grain size in the film will be < 0.5 μm. This is confirmed by SEM observations of several fracture crossections. The dramatic broadening and height reduction of the dielectric constant peak as a function of temperature is also consistent with a grain size reduction to below a micron, particularly a reduction in the grain to grain boundary volume ratio. These microstructure changes limit extrinsic contributions to dielectric permittivity as reported by Randall et al. (**20**).

The lack of a significant increase in the dielectric constant with poling is also consistent with a strong clamping of the film which prevents domain re-orientation during poling. If this extrinsic effect is clamped out it is possible to describe the piezoelectric effect in terms of intrinsic material properties. Using the intrinsic relationship between the remnant polarization – P_3, dielectric permittivity – ε_{33} and piezoelectric coefficient – d_{33},

$$d_{33} = 2Q_{11}P_3\varepsilon_{33} \qquad \text{Intrinsic Piezoelectric Effect} \qquad [5.7]$$

the electrostrictive coefficient - Q_{11} for the film is 0.037 m^4C^{-2}. This value is the same as calculated by Haun (**21**) for a polycrystalline 52/48 PZT using single crystal data and a parallel mixing rule. This result lends support to both the relative accuracy of the d_{33}

measurement and the theory that the lateral clamping of the substrate prevents domain re-orientation even at a thickness of 13 μm.

There were several other phenomena associated with these films on Ag/Pd that were not consistent with the bulk, or accounted for by a simple grain size or clamping effect. The dark brown color of the film is consistent with reduction of lead in the PZT. The asymmetry of the hysteresis loops appears to be due to an asymmetric contact potential.

Because of the possibility that these non-ideal behaviors could be a result of gold-Ag/Pd electrode asymmetry, silver migration into the film, and/or palladium oxidation/reduction, the next step taken was to form films on a platinum bottom electrode which could then have symmetric platinum electrodes sputtered on top.

Table 5.2 PZT Bulk and Film Properties

	Bulk Samples	Film on Silver/ Palladium #81	Film on Platinum #120	Film on Platinum #142
Thickness	1,370 μm	13.5 μm	5.5 μm	8.5 μm
Dielectric Constant. Maximum -Unpoled	1,227	920	980	800
Dielectric Constant, Average - Unpoled	1,157	854	815	712
Standard Deviation	*7%*	*8%*	*12%*	*9%*
Increase in Dielectric Constant with Poling, Max	61%	5%	-3.5%	-5.6%
Ave. Dielectric Loss, Tan δ	0.015	0.049	0.038	0.035
Remnant Polarization Maximum	36.5 μC/cm^2	27.5 μC/cm^2	32.2 μC/cm^2	33.1μC/cm^2
Remnant Polarization Average	35.3 μC/cm^2	16.6 μC/cm^2	24.7 μC/cm^2	28.3 μC/cm^2
Standard Deviation	*N/A*	*24%*	*11%*	*8%*
Coercive Field, Average	17 kV/cm	18.7 kV/cm	17.4 kV/cm	26.1 kV/cm
Standard Deviation	*N/A*	*23%*	*8.5%*	*11%*
Piezoelectric Coefficient, d_{33} Maximum	406 pC/N	140 pC/N		128 pC/N
Pyroelectric Coefficient, *p* @ 25°C	45 nC/cm^2°K			25 nC/cm^2°K
Electrostrictive Constants, Q_{11}	0.037 m^4/C^2	0.037 m^4/C^2		0.043 m^4/C^2
Dielectric Peak Height/Width	50/19°	11.5/122°	14/93°	8/110°
Sintering - Rise Time/Peak Temperature/Hold Time (min./°C/min.)	300/1,270°/ 120	45/900°/30	64/900°/12	45/950°/5

5.4.4.3 Platinum Screen Print Electrodes

Platinum Electrode Preparation — A single screen printed layer of platinum after sintering had a visually rough surface and when examined by SEM showed many through thickness pores from 1 to 10 μm. To produce a smooth, continuous electrode the platinum was screen printed, sintered, and polished, and the process repeated three times to assure a continuous, pore-free surface. The electrodes were sintered at 1,250° for 30 min. with a 40 min. rise time. The final polishing then brought the surface to a mirror finish. The resulting electrodes were 5 to 10 μm thick.

The electrical properties of two films on Pt electrodes are summarized in Table 5.2. The first, # 120 with a calculated thickness of 5.5 μm was characterized only for dielectric and polarization properties. The second, # 142 with a measured thickness of 8.5 μm, showed a slightly higher average density and was characterized for piezo and pyroelectric properties as well.

Sintering on Pt Electrodes — The first set of depositions on Pt electrodes was sintered with and without added lithium and a target of 20 vol. % lead oxide. The films were then sintered at 900°C for 20 min.

The resulting films showed very uneven sintering behavior. A large part of this appeared to be due to the uneven distribution of the excess lead oxide. When the lead acetate solution dries the lead acetate appears to migrate with the drying front. The areas that dry first end up with very little lead acetate while the final areas to dry end up with an excess. The film with the highest density also had the highest addition of lithium. The films without lithium showed areas with almost no sintering and were still the yellow color of the deposited powder. At the uncoated edges of the substrate there were rough, colored spots which were assumed to be due to interaction between the excess lead oxide and the platinum electrode.

Preparation of Film #120 — A second set of eight films was deposited from a suspension consisting of 2.03 g PZT in 91.1 g of acetic acid. The suspension was prepared one day, used to deposit one substrate at that time, and then used for deposition of the rest twenty four hours later. The suspension was both dispersed and re-dispersed the next day by sonication while stirring for two minutes. Twelve depositions were made with four rejected due to non-uniformity or non-adherence of the deposition to the substrate. Of the good depositions, four were deposited at 250 V and four at 500 V. The suspension was stirred between depositions but was not re-sonified.

Film #120 was deposited one hour after sonication. It was deposited at 500 V for 80 sec. which gave a current density of 60 μA/cm^2 and yielded a deposition of 3.9 mg/cm^2.

The film was doped with lithium by re-wetting the deposition with lithium acetate solution to yield 4.3 mol. % lithium oxide. To obtain a better distribution of lead oxide in the deposition, a spray atomiser was used to spray the lead acetate solution onto the deposition. The amount of lead acetate added was determined by weight after drying of the solution, and after oxidation would yield a 10 vol. % lead oxide in the deposition. This was the highest lead addition in this set of depositions. The film was sintered at 900°C for 12 min. with a rise time of 64 min.

The resulting film was generally a light sea green in color with two irregular patches of darker green near the top and bottom edges. The uncoated edges of the substrate showed no deterioration of the platinum electrode.

Properties of Film #120 — This film showed the best uniformity and continuity of the films produced here. The top surface was sputtered with 37 2.15 mm dia. circular platinum electrodes in seven rows. All of the electrodes were good and showed a dielectric loss of less than 0.06. It was also possible to test the polarization hysteresis with a peak voltage 40 V on all of these electrodes without breakdown of the film. This indicates a very low density of pinholes and cracks in the sintered film.

Based on the weight/area of the deposition, the thickness of the film at 100 % density would be 4.9 μm. An arbitrary density of 90 % was applied, giving an estimated thickness of the film of 5.5 μm. This was used for calculating the dielectric constant and electric field figures.

The values for this film are listed in Table 5.2. The dielectric constant was measured with a 1 kHz sine wave input with a 10 mV peak voltage. This gives a maximum voltage field of 18 V/cm. Hysteresis was measured with a 15 Hz sine wave input with a 40 V peak. Hysteresis loops were symmetric and there was no difference between positive and negative polarizations or coercive fields beyond the limits of experimental error. With the film polarized by the polarization measurements the dielectric constant was re-measured. This showed an average decline of 3.5% while the dielectric loss declined from 0.038 to 0.026.

The temperature/capacitance curve showed a higher peak than the film on silver/palladium with a peak 14 times the 25°C value occurring at 374°C. The half height width is slightly lower at 93°C.

The darker areas of the film corresponded to the electroded areas with the highest capacitance and polarization. This is consistent with these areas having the highest density.

Preparation of Film #142 — This film was one of a set of ten deposited from a suspension of 3.0 g PZT in 142 g acetic acid. The film was deposited 11 hours after the suspension was first prepared and was the seventh film deposited from this suspension. The suspension was stirred while sonicating for 2 min., then allowed to settle for 7 min. prior to the beginning of deposition. The film was deposited at 250 V for 2.5 min. giving a current density of 34 μA/cm^2, and a final deposition weight of 6.6 mg/cm^2.

In an attempt to improve the distribution of the sintering additives a solution was prepared in which both lithium and excess lead could be added to the deposition by spraying. A solution of 25 wt. % lead ethylhexanoate in methyl ethyl ketone was prepared. Dry lithium acetate added to this solution did not dissolve. To dissolve the lithium acetate a few drops of methanol were added to the solution. This resulted in the immediate formation of a substantial quantity of a white precipitate. These precipitates then re-dissolved with sonication. This solution was stable for long enough to spray onto the depositions, but formed another precipitate one day later which did not redissolve.

This solution was sprayed onto the deposition in several coats that were allowed to dry between sprayings. The amount added to the deposition was controlled by weighing after each coat had dried. This procedure was not entirely successful. It appeared that later sprayings would re-dissolve the earlier coats causing migration of the lead organic to areas of higher concentration during drying.

Prior to sintering, the depositions were heated to 450°C at 1°/min. in air to burn out the organic compounds. The lead component burned to red lead oxide, giving the deposition a reddish color. This was visibly non-uniform across the deposition confirming the uneven distribution of the lead organic after spraying.

The final quantity of added lead oxide was 12 vol. % and lithium 5 mol. % of the deposition. This was determined by the weight of lead oxide after burnout and the lead/lithium ratio in the spray solution.

The film was sintered in a sealed crucible at 950°C for 5 min. with a 45 min. rise time. A temperature check ring placed underneath the crucible showed a peak temperature of 890°C, therefore the actual peak temperature experienced by the film will be between this and the 950°C measured by the furnace thermocouple.

Properties of Film #142 — Five electrodes were initially sputtered onto the film surface, and initial tests of polarization and capacitance were made. The surface was then polished with 1 μm diamond paste to remove the first electrodes. The film was then sputtered with a new set of 49 electrodes in 7 rows. 13 electrodes were bad, showing either a short circuit or a dielectric loss of more than 0.10.

Fig 5.33 below shows a polished crossection of the film with a thickness of 8.5 μm. This thickness was used for all electric field and dielectric constant calculations below. The theoretical uniform 100% dense thickness based on deposition weight is 8.3 μm. The density of the film at this point determined by graphical analysis of the SEM image is 87%.

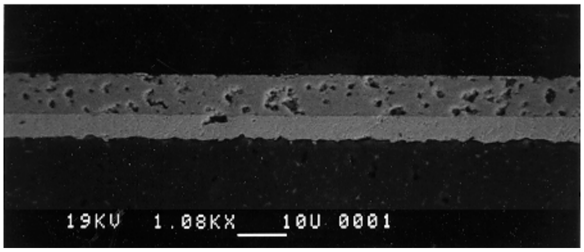

Fig. 5.33 Cut and polished crossection of PZT film. The layers from the top are: 8.5 μm PZT film; 5 μm Pt electrode; and alumina substrate.

Capacitance was measured with a sine wave input at 1 kHz with a 10 mV peak voltage. This gives a electric field of 12 V/cm. The average dielectric constant is 712 with an average loss of 0.035 and a peak dielectric constant of 800 measured at three electrodes. After the film was polarized by hysteresis measurements below, the average dielectric constant declined by 5.6% while the average loss dropped to 0.027. The changes in dielectric constant with polarization ranged from +3% to -7%.

The temperature/capacitance curve, Fig. 5.34, showed a lower peak than the film on silver/palladium with a peak 8 times the 25°C value occurring at 387°C. The half height width is also slightly lower at 110°C. The location of this peak is likely shifted to a higher temperature by the rapid rise in loss in this temperature range.

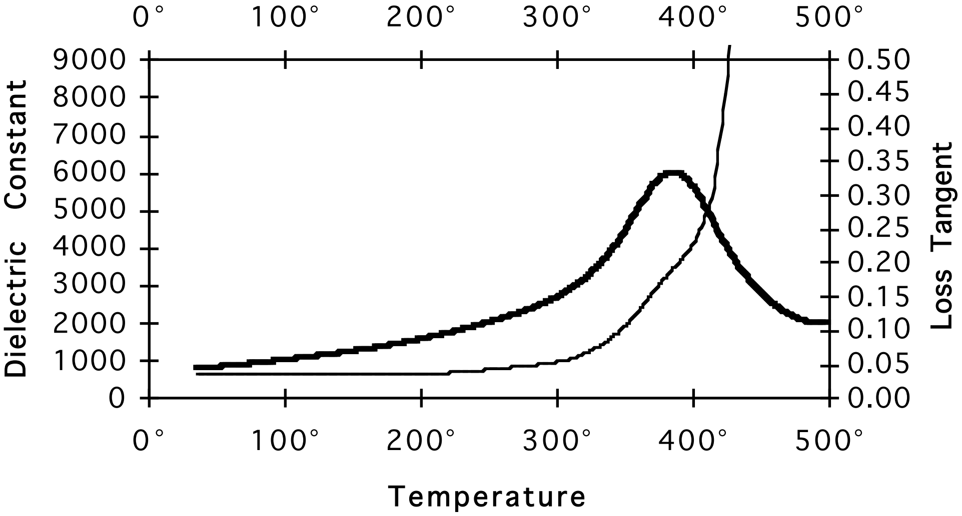

Fig. 5.34 Capacitance as a function of temperature for film #142 at 1 kHz 12 V/cm. Dielectric peak occurs at 387°C.

Polarization hysteresis was measured with a 60 Hz sine wave input with a 100 V peak voltage which results in a field of 118 kV/cm. The average remnant polarization was 28.3 μC/cm^2, with an average coercive field of 26.5 kV/cm. The highest measured was 33.6 μC/cm^2. This hysteresis loop is shown in Fig. 5.35. The hysteresis loops were symmetric with no significant or systematic differences between positive and negative polarization and coercive field. Raising the maximum voltage to 150 V, 177 kV/cm, increased the measured average remnant polarization to 30.7 μC/cm^2 and average coercive field to 29.4 kV/cm. Remnant polarization declined with cycling. Seven electrodes were taken through thirty polarization cycles with a 150 V peak. They showed an average decrease in P_r of 8.6%, with a maximum reduction of 15% and minimum of 1.1%. Three electroded areas were taken through 300 polarization cycles resulting in decreases in polarization of 13, 20, and 4.4%. This polarization fatigue was accompanied by an increase in coercive field of 9, 8, and 11%, respectively.

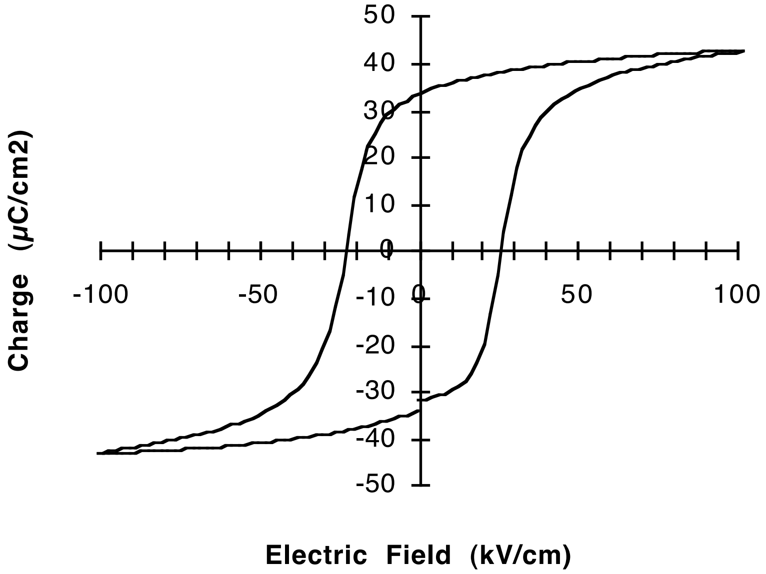

Fig. 5.35 Polarization hysteresis with P_r of 33.6 μC/cm2 and an E_c of 24 kV/cm.

The pyroelectric coefficient of 25 nC/cm^2°K at 25°C was determined by cooling and re-heating a portion of the sample over a range of ±125°C at a rate of 4°C/min. Prior to measurement the film was poled by the application of a 100V potential for one minute at room temperature. Remnant polarization measured on this portion of the sample was 30 μC/cm^2.

When attempting to measure the pyroelectric discharge of this sample it exhibited an anomalous discharge behavior similar to that seen with the film on a silver/palladium electrode above. The film was heated 425°C at 6°C/min. Between 250 and 400°C the positive current from the sample was approximately 30 times the measured remnant polarization.

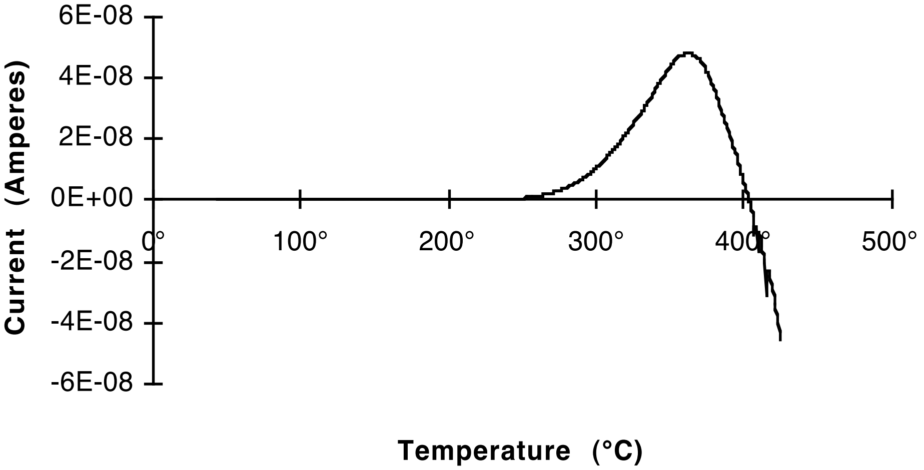

Fig. 5.36 Pyroelectric discharge.

When measuring the d_{33} coefficient of these films it is essential to eliminate bending modes in the substrate. Bending can easily generate much higher in-plane strains in a film on a substrate than are possible to produce orthogonally even with great effort. When placing the electroded substrate into a standard Berlincort meter, it is possible to generate wildly varying readings from negative to positive. Bending mode vibration of the substrate will produce a current due to the d_{31} in-plane compression of the film that will completely swamp any d_{33} current from orthogonal compression of the film.

To eliminate these bending modes a 4.14 mm disk was cut from the film and substrate with a single electrode in the center. 1.65 mm disks cut from an alumina substrate were then attached to the top and bottom of the film disk with crystal bond adhesive. When properly electroded this assembly could be mounted directly in a Berlincourt meter. Because of the low aspect ratios and flat polished surfaces of the elements of this stack bending should be minimized. Because of the small size and mass of the center disk, vibrational bending modes should be eliminated at the frequency of the Berlincourt meter. A crossection view of this stack is shown in Fig. 5.37 with aspect ratios drawn to scale.

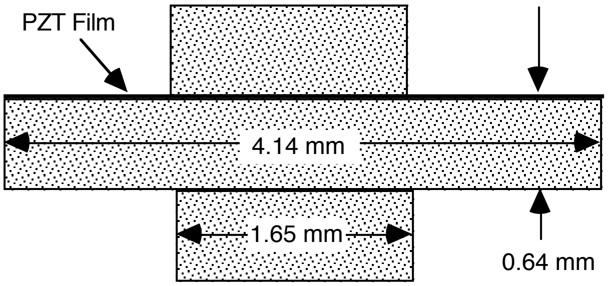

Fig. 5.37 Low aspect ratio stack to minimize bending modes in measuring d_{33}.

Using this assembly a series of polarizing voltages were applied to the film and the piezoelectric coefficient measured. The voltages in 10 V increments from 5 V to 75 V were applied for one minute to the film. The resulting d_{33} hysteresis loop is shown in Fig. 5.38.

During poling at 55 V and above there was a measurable current which rose for the first 20 to 30 sec. and then stabilized. The current was not linearly related to voltage, appeared to be time dependent and was slightly higher when the top electrode was positively polarized. In the final polarization reversal performed on this sample, voltages of -65 and -75 V induced steady currents of -3 and -10 μA, and voltages of +55, +65 and +75 V induced currents of +2, +6 and +10 μA, respectively. Polarization hysteresis measured at this electrode prior to preparing it for the d_{33} measurement was symmetric with a P_r of 30 $\mu C/cm^2$ with a coercive field of 27 kV/cm. After testing, the polarization hysteresis showed a 40% difference between positive and negative coercive fields, having P_r's of -25.0 and +26.2 with coercive fields of -28 and +20 kV/cm.

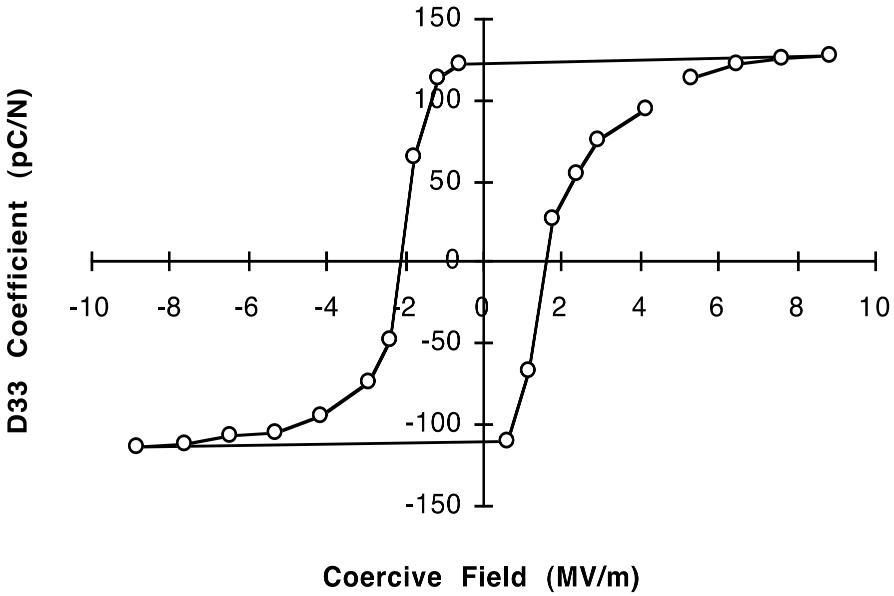

Fig. 5.38 Piezoelectric coefficient hysteresis.

Discussion — The uniformity of both the deposition and addition of sintering aids still needs to be significantly improved. Non-uniformity in deposition and drying is the likely cause of cracks and pinholes in the sintered film which caused 11 of the 49 electrodes to show a short circuit when tested. Non-uniform thickness of the deposition and distribution of sintering aids are likely causes for the relatively high standard deviation of dielectric properties of 9%.

A temperature check ring placed underneath the sintering crucible showed a significantly lower temperature than the programmed peak temperature for the furnace. In the sintering of film #120, a different furnace was programmed for 30 min. at 900°C, but an actual recording of the temperature showed a significant lag in the furnace temperature so that it was only at 900°C for 12 min. Placing a thermocouple inside the sintering crucible would significantly improve control of the sintering process.

The electrostrictive coefficient Q_{11}, calculated from eq. [5.7], is 0.043 m^4/C, which is within the predicted range in (**21**). This, along with the very simple method of measurement, supports the reasonableness of the d_{33} values.

In comparison to the film on silver/palladium, #81, this film showed a lower dielectric constant, dielectric loss, d_{33} coefficient, and dielectric temperature peak, with a higher remnant polarization and coercive field. This set of differences could be accounted for if film #142 had a slightly higher density and a significantly smaller average grain size than film #81.

There are several ways that this could occur. There are different sintering conditions, different sintering additive levels, the electrode material and deposition conditions. Film #81 was held at temperature longer than film #142 which may have allowed for more grain growth. However, previous sintering comparisons on this system showed grain size was only related to the maximum sintering temperature, and there was very little effect of sintering time up to two hours. Film #81 had twice as much lead oxide and half the lithium added for sintering than was added to film #142. Experiments have shown that lithium strongly promotes grain growth while excess lead oxide primarily aids consolidation with significantly less grain growth. Given this, the expectation would be that #81 would have a smaller average grain size than #142. The unknown component in this comparison is the electrode material. Silver/palladium has been shown to affect the sintering of PZT. Clearly, the dramatic difference in film color between the film on Ag/Pd and Pt show that there is some interaction with the Ag/Pd electrode material, however, whether this significantly affects grain size at this sintering temperature is unknown. Finally, there are the deposition conditions. Prior to deposition both suspensions were stirred while sonicating to redisperse the PZT powder. The deposition conditions were very similar, 250 V for 90 sec. for film #81 and 300 V for 150 sec. for film #142. The key difference is the settling time between the end of stirring and the beginning of deposition. This was exactly 2 min. for film #81 and 7 min. for film #142. In both cases the sedimentation speed of 3 μm particles and larger would be higher than their electrophoretic mobility in the applied field and these particles would not be incorporated into the deposition. The difference is the extra sedimentation time would virtually eliminate any particles in the 1.5 to 2.5 μm range that might be incorporated into the deposition with a shorter sedimentation time. Given previous observations of the equilibrium grain size for lithium and lead fluxed sintering in this temperature range, the incorporation of particles in the 2 μm size range could significantly raise the average grain size in the sintered deposition.

There are a number of factors that point to some sort of electrochemical polarization of the film under high voltage. These are: the anomalous pyroelectric discharge, the non-ohmic current at high voltage fields, imprint, polarization fatigue, and the increase in coercive field with repeated polarization reversals. The presence of this anomalous pyroelectric discharge in films on both types of electrode indicates that at least one component of this effect is unrelated to interactions with the silver/palladium electrode.

The pyroelectric coefficient, p, is the change in polarization, $\boldsymbol{P}$, with temperature:

$$p = \frac{\partial \boldsymbol{P}}{\partial T} \qquad \text{Pyroelectric coefficient} \qquad [5.8]$$

The pyroelectric coefficient of the film is only 60% of that of the bulk sample, even though the polarization is 86% of the value for the bulk sample. This is counterintuitive given that the thermal expansion of the alumina substrate is much higher than that of the PZT film. The expansion of the substrate should cause a larger lateral expansion in the film that in the bulk sample. This expansion would add a piezoelectric component to the pyroelectric current. However, given the much lower permittivity of the film compared to the bulk, the average internal electric field of the film is 2.2 x that of the bulk. Based on the measured thermal coefficients of polarization and capacitance, the ratio of the thermal coefficients of internal electric field is 2.9, and the ratio of absolute change in internal field in the film compared to the bulk is 6.3. The much larger reduction in internal field in the film leads to a reduction in the electrostrictive stress on the film. This causes an expansion of the material in the polarization direction which, through the piezoelectric interaction, reduces the measured pyroelectric current.

5.4.5 Conclusions on the EPD of Complex Lead Perovskites

The conclusions in this section are broken down into three sections from most specific to most general. The first is a description of the nature of the PZT films formed so far, how they could be improved, and what resulting improvements in properties might be expected. This is followed by recommendations for how the EPD and sintering of these films could be changed to achieve these film quality improvements. Finally are general conclusions about the EPD of complex compounds.

Intermediate thickness PZT films – Because of the mismatch in thermal expansion coefficients between PZT and the alumina substrate, these films are highly compressed in the plane of the film. An unconstrained, unpoled, niobium doped PZT has an isotropic thermal contraction of less than 0.05% from the curie temperature to room temperature (≈350°C). Over the same temperature range the alumina substrate will contract by 0.29%. This imposes an excess in-plane strain on the film of -0.25%. This compression forces the ferroelectric domains to align perpendicular to the film. This mechanical domain orientation allows the relatively high polarizations achieved here. Because the domains are aligned almost entirely by the clamping of the substrate, poling does not induce any additional domain alignment and there is no significant change in the dielectric constant.

The most significant difference between these films and the bulk ceramic is the dielectric constant, with a poled dielectric constant of 1,850 for the bulk sample and film constants mostly in the 700 to 900 range. There are three primary sources for this difference, porosity, clamping of extrinsic contributions and low dielectric constant grain boundary phases. Porosity alone can only explain part of the difference. Using the dielectric mixing law, eq. [5.9] where ϕ_p is the volume fraction of randomly dispersed pores, and ε_m is the measured dielectric constant, the dielectric constant of the fully dense material, ε_d, can be calculated.

$$\varepsilon_d = \varepsilon_m \left(1 - \frac{3\phi_p}{\left(2 + \phi_p\right)}\right)^{-1} \qquad \text{Dielectric Mixing for Randomly Dispersed Pores} \quad [5.9]$$

For the bulk sample with a measured dielectric constant after poling of 1,850 and a density of 97%, the fully dense dielectric constant would be 1,930. For film #142 with a density of 86% and a measured ε of 700, ε_d, is 870, still only 45% of the bulk sample. Given the similarity of polarization, coercive field and dielectric constant maximum temperature, there is undoubtedly a large component of the film which retains the properties of the Nb-doped PZT starting material. This means that either the dielectric response of the intragranular material is suppressed by the strong lateral compression, or there is a significant amount of very low permittivity grain boundary phase. Most likely it is some combination of the two.

To the extent that this reduction in permittivity is due to suppression of extrinsic contributions caused by clamping and compression of the film by the substrate, there is little that can be done other than to change or remove the substrate. This is discussed further below.

The issue of grain boundary phases ties in with one of the other significant differences between these films and the bulk ceramic, the relatively high conductivity of the films. There are several issues that could have a bearing on the nature of both conduction and grain boundary phases in these films. The niobium doping of the PZT is, in part, intended to compensate for A-site vacancies that occur during the high temperature sintering of the bulk ceramic and in that case yields a very low conductivity material. In contrast the films are sintered at low temperature in the presence of large amounts of excess lead oxide, which raises questions about the density of lead vacancies to be compensated. The excess lead oxide presumably aids the sintering of the film by allowing the dissolution/precipitation of titania and zirconia from small grains to larger grains. However, zirconia has a lower solubility in lead oxide than titania. This raises the possibility that grains in these films are surrounded by a double shell. The inside shell zirconia rich and the outer shell titania rich, both having much lower dielectric properties than the stoichiometric composition. Finally, there is the added lithium. Based on observed morphology changes in sintering it appears that the primary effect of lithium during sintering is to speed surface diffusion. However, whether lithium ends up concentrated in the grain boundaries or diffused throughout the sample is not known. The low oxidation-reduction potential and small size of the lithium ion does make it one of the first factors to investigate in relation to the conductivity and electrochemical polarization of the films.

The issue of grain boundary phases, conductivity, electrochemical polarization and fatigue in these films all have the potential to be addressed by changes in doping and sintering conditions. To the extent that the relatively low permittivity of these films is due to grain boundary phases, better understanding of these phases can allow them to be minimized, giving a proportionate rise in permittivity. If it is these phases which are the primary cause of the difference in dielectric constant between the film and the bulk, and not the clamping effect of the substrate, permittivities approaching that of the bulk ceramic should be possible.

With polarizations and electrostrictive coefficients similar to those of the bulk ceramic, if the permittivity of the film could also be raised to a value similar to that of the bulk, the piezoelectric and pyroelectric coefficients should follow suit. It is not unreasonable to predict piezoelectric d_{33} coefficients of 300 pC/N or higher. Because of the higher thermal expansion of the alumina substrate, pyroelectric coefficients for the film on the substrate may actually be higher than that of the bulk.

However, for many uses these films will need to be separated from the substrate. The in-plane strain in the film due to the larger thermal contraction of the substrate is -0.25%, while the residual strain in a bulk ceramic due to the alignment of domains during poling is -0.12%, perpendicular to the poling direction. This leaves an additional -0.13% strain in the clamped film. How this additional strain manifests itself in the film will have a dramatic effect on the properties of the film when it is removed from the substrate. This excess strain could result in a greater domain orientation than is possible with only electrical poling. In this case, when the film is released from the substrate, the remnant polarization may drop dramatically, possibly with a further drop in dielectric constant. This would result in a film with very poor piezoelectric properties. On the other hand, if this excess strain results primarily in elastic deformation of the film and not domain orientation beyond what would occur during poling, the release of this film could result primarily in unfreezing domain wall motion. This could result in a substantial increase in the dielectric properties without a substantial loss in polarization. In this case the released film could have properties approaching those of the bulk ceramic. Determining which of these is the actual case is one of the most immediate and interesting tasks to undertake from the rather long future work section of this thesis.

EPD and Sintering of PZT — The following are comments and suggestions further improve the reproducibility, uniformity and properties of these films

- Suspension/deposition — The possibility of depositing this material using the Ion Depletion Enhanced Electrostatic deposition method was shown in §5.4.3.2. If it is possible to do this from a colloidally and chemically stable suspension this would likely lead to a major improvement in uniformity of film thickness and homogeneity of particle packing. The electrostatic deposition method used here has no compensating mechanism for thickness variation, therefore any non-uniformities in cell geometry or convective flows will lead to thickness non-uniformities in the film. Ion depletion enhanced deposition will also consolidate the particles to almost full random packed density prior to drying. This should lead to more uniform particle particle packing and lessened incidence of cracking during sintering.

- Electrode — Forming the bottom electrode by screen printing and polishing is both time consuming and expensive. As was shown in §5.2.4, this type of electrode could be produced by EPD and sintering. However, this two step process may only have an advantage for alloy or composite electrodes. For single metals, such as platinum, simple electrodeposition is a well known commercially available process which produces a dense electrode without further processing.
- Doping/sintering additives — The largest problem in forming these films is the uniform and accurate distribution of the sintering additives. While better spraying solutions and procedures may help this in the short run, the ultimate solution to this mixture problem will be to precipitate the desired sintering additives onto the surface of the particles prior to deposition. It is not an unreasonable goal to develop a coating which contains sintering additives and dopants, prevents dissolution of the particles and provides surface charge for stabilization and electrophoresis.
- Pyroelectric Measurements — The anomalous pyroelectric discharge in these samples is both interesting and unexplained. It is very likely that the mechanisms involved in this will be related to the mechanism of fatigue and aging in these films.

EPD of Complex Compounds — Based on the objectives outlined in the beginning of this section this demonstration has to be considered an unqualified success. When adjusted for grain size and the clamping of the substrate, the films showed a full set of properties that match properties of bulk samples prepared from the same starting powder.

5.5 Deposition of Titania

The deposition of titania is included here to demonstrate another system in which IDE deposition is achieved and to provide a graphic demonstration of the automatic leveling effect inherent in IDE deposition. There are two parts to this section. The first part is a demonstration to show that deposition of titania from this system is occurring by the IDE mechanism. The second part compares the electrostatic deposition of PZT with no inherent leveling effect with the automatic leveling effect inherent in the IDE deposition of titania.

5.5.1 Materials

TiO_2 — The titania powder used in these experiments is High Purity grade from Ishihara chemical company. The powder particles are close to equiaxed with an aspect ratio of less than 2, as shown in the accompanying photograph.

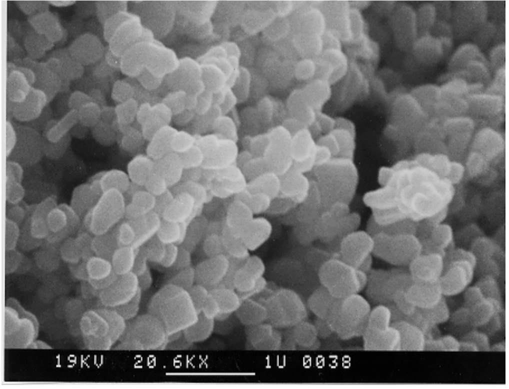

Fig. 5.39 Titania powder.

The powder was determined to be phase pure rutile by powder X-ray diffraction. The BET surface area was 7.4 m^2/g, giving an equivalent spherical diameter of $0.2\mu m$. An average particle diameter of $0.3\mu m$ was determined by centrifugal sedimentation light scattering (Horiba CAPA-700 Particle Analyzer). The powder was washed in de-ionized water until 100g of powder mixed with 400g of de-ionized water at room temperature produced a conductivity increase of less than 0.05 $\mu S/cm$ in the wash water. The powder was dried at 78°C, and equilibrated at 28°C, 30% relative humidity.

Ethanol — The suspensions were made using USP Grade Ethyl Alcohol from Pharmco Inc., Brookfield, Massachusetts, USA. Water content was determined to be 0.07 wt.% by Fisher titration.

Iodine — Iodine used was 99.8% ACS resublimed flakes. A stock solution of 0.5 wt.% iodine in ethanol was prepared and kept on the shelf for preparation of the deposition suspensions.

Substrates — Substrates used were Coors Ceramics alumina electronic thin film substrates, ADS 995 or better. These are 99.5% Al_2O_3 with a grain size of ≈ 1 μm. The substrates were electroded by sputtering with copper for three minutes followed by platinum for six minutes. The electrodes were then annealed at 850°C for ten minutes. The final thickness was 300 to 500 nm.

5.5.2 Suspension, Deposition and Sintering

The deposition conditions for the 10 micron film shown below were as follows:

Suspension — The suspension was mixed as follows: As-recieved ethanol; 0.34 vol. % TiO_2 powder; Iodine: 0.031 wt.%. The powder was dispersed using a Branson Sonifier 350 at 70% setting for four minutes while stirring. Two hours later, the suspension was re-sonified for two minutes. Final conductivity was measured as 13.5 μS/cm.

Deposition Conditions — A constant current of 0.64 mA/cm^2 was applied for 60 seconds between two electrodes spaced 2 cm apart.

Sintering — The deposited film was sintered at 1,250°C in air. The firing schedule was: heating at 10°C/min. to 1,250°C, 5 minute hold at 1,250°C, and cool down at 20°C/min.

5.5.3 Results

During the constant current deposition the voltage showed a linear voltage rise of 27V over the 60 sec. deposition time. This is shown in Fig. 5.40. The green thickness was not measured for this deposition, however, based on similar depositions the estimated green thickness is expected to be 17 to 19 μm.

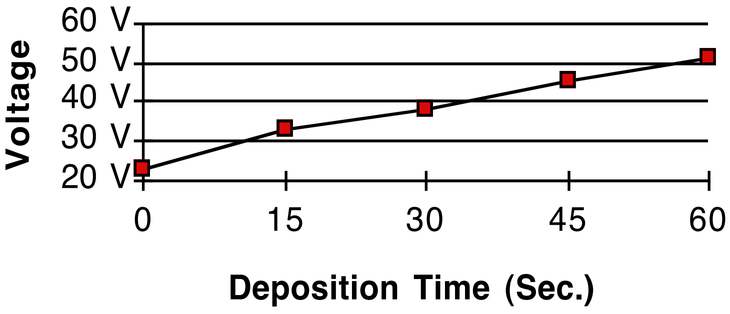

Fig. 5.40 Voltage rise during constant current deposition of titania.

Fig. 5.41 (a) shows a fracture surface crossection of the film formed by the process above. The TiO_2 grainsize is ≈ 10μm. The film is highly adherent, smooth and optically transparent.

Fig. 5.41 (b) shows a fracture surface crossection of a deposition formed by the same process as above. In this case the suspension used above was allowed to stand overnight. The conductivity was elevated by approximately 30%, possibly due to metal ion contamination. This lead to a slightly lower voltage rise of 17 V over the course of the deposition at the same current density, but is otherwise identical to the deposition above. This picture is included to illustrate the uniformity of the unsintered deposition achieved using this method.

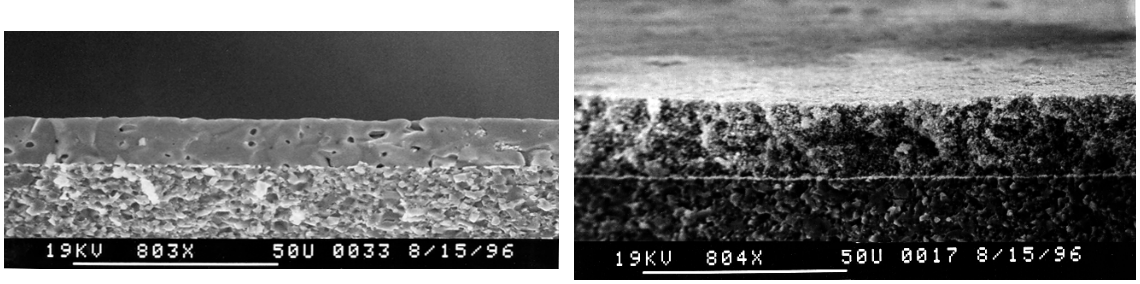

(a) (b)

Fig. 5.41 (a) 10 μm TiO_2 film with no through thickness porosity on an Al_2O_3 substrate sintered @ 1,250°C. Deposition Time: 60 sec.@ 0.64mA/cm^2 (b)18 μm unfired deposition of TiO_2 particles on an Al_2O_3 Substrate.

5.5.4 Deposition Conclusion

The observations above can be considered proof of deposition by the ion depletion enhanced electrostatic deposition mechanism. The stability and conductivity of the suspension is improved by the addition of iodine. This is likely due to the iodine reacting in the ethanol to form iodic acid (HI) in a similar manner to what was proposed in §5.4.3.2. This acid then increases the positive surface charge on the particles in the same manner as HCl was shown to increase the surface charge on alumina in Ch. 3. With no change in the bulk suspension conductivity, the voltage rise in the system must be concentrated across the depositing layer. The voltage rise of 27 V across an 18 μm deposited layer gives an average voltage gradient across the layer of 1.5 x 10^6 V/m. This can best be accounted for by positive ions in solution being consumed at the cathode creating an ion depleted layer which is stabilized by the depositing layer of particles.

5.5.2 Deposition Comparison

To test the automatic levelling effect inherent in ion depletion enhanced deposition two depositions were made in systems having distinctly non-uniform bulk electric fields, one using simple electrostatic deposition, the second using the IDE effect.

To create the non-uniform electric field a short conductive post was attached to the center of the same flat substrates used for other depositions made above. In a uniformly conductive medium the electric field lines will tend to concentrate on the corners of the post, as shown in Fig. 5.42. If particles simply follow these field lines they will accumulate at the corners of the conductive post.

(Note: These depositions were performed vertically upward with positive particles depositing on the cathode at the top of the cell and the post pointing down. Fig.s 5.42-5.44 are shown inverted for clarity.)

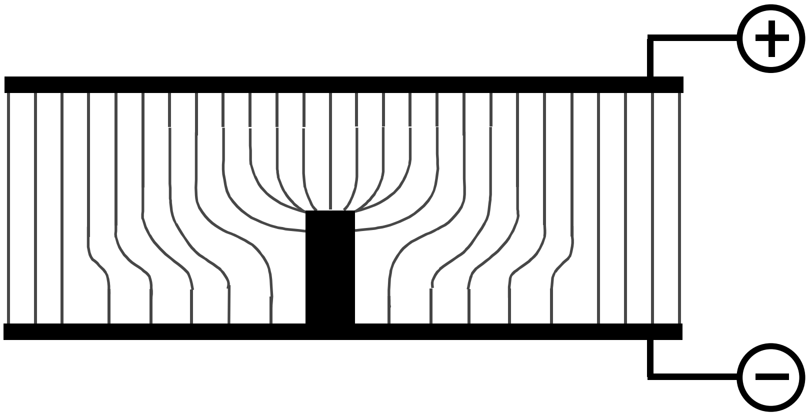

Fig. 5.42 A conductive post in an uniformly conductively medium will concentrate electric field lines at the corners of the post

A deposition of PZT on a post illustrates the non-uniform field effect on deposition in the absence of the automatic levelling effect. The post is a polymer/graphite rod attached to a substrate by a drop of epoxy. The assembly is sputtered with platinum from two angles to assure uniform conductivity over the surface of the post. The PZT powder was deposited from acetic acid as detailed in §5.4.3.4. A constant voltage of 300 V was applied with an average 2 cm electrode spacing. The resulting deposition was removed from the deposition bath and allowed to dry in air. The resulting deposition is shown in Fig. 5.43. This clearly shows the formation of a 'crown' deposition around the edges of the post. The deposition also thins along the length of the post with almost no deposition occuring around the base of the post where the electric field will be the lowest.

This 'crowning' behavior is shown to be dramatically reduced in the case of the IDE depositon of titania. In this case the post is a copper wire also attached to a substrate with epoxy and sputtered with platinum to provide an electrical connection from the surface of the substrate across the epoxy to the copper post. The exact deposition conditions were not recorded, however the titania was deposited from an ethanol/iodine suspension with an initial voltage of ≈ 20 V which showed a linear rise during deposition. This linear voltage rise being characteristic of IDE depostion. The resulting deposition is shown in Fig. 5.44.

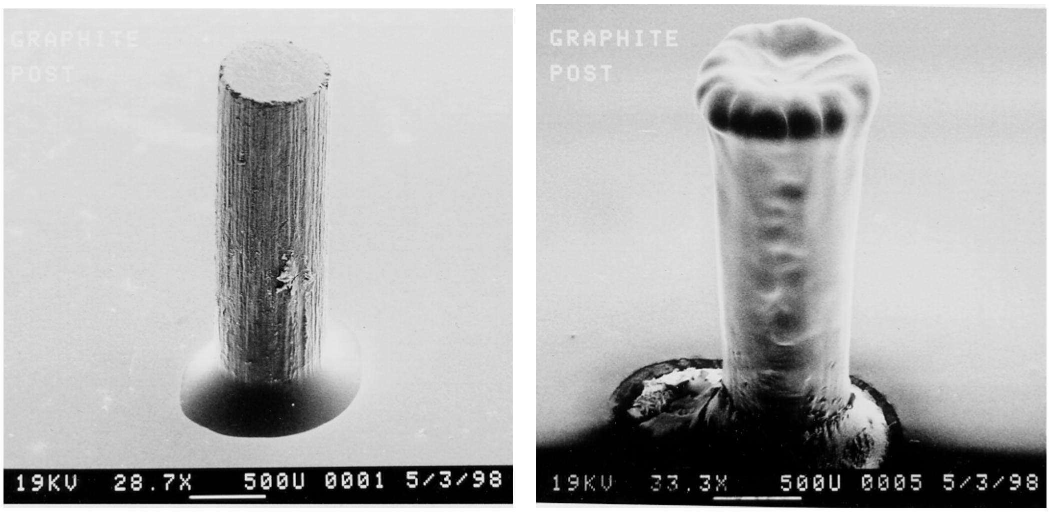

(a) (b)

Fig. 5.43 (a) Graphite post on an alumina substrate sputter coated with platinum to provide uniform conductivity. (b) Graphite post after direct electrostatic deposition of PZT.

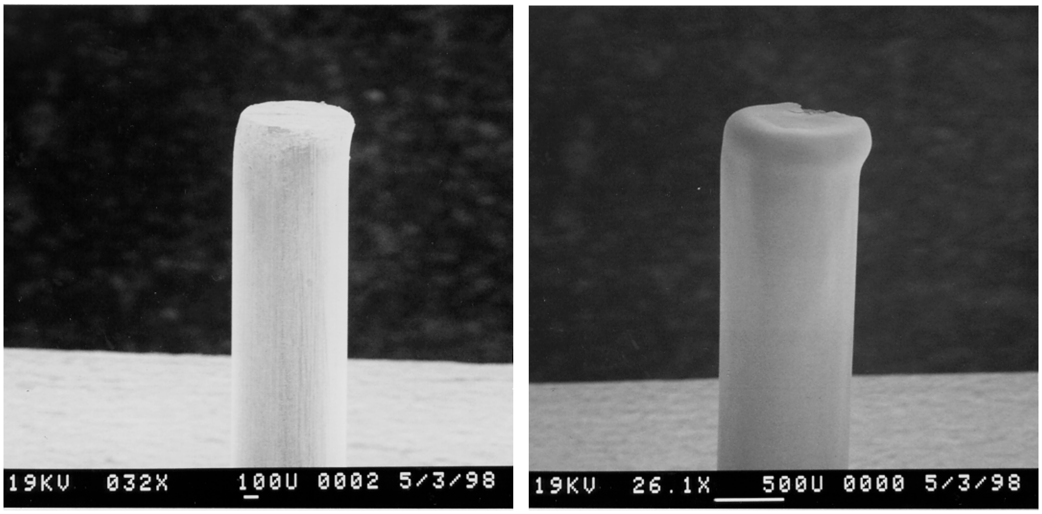

(a) (b)

Fig. 5.44 (a) Copper post. (b) Copper post after deposition of TiO_2.

It can be seen that while there is some thickening of the deposited layer around the corners of the post, the coating is generally uniform. With a voltage gradient in the range of 1 V/μm in the deposited layer, a slight thickening of the deposition can lead to a large reduction in the voltage at the surface. This regulation of potential around a surface can compensate for very large initial inhomogeneities in the bulk electric field.

5.6 Conclusion

In the first chapter several possible advantages for processing by EPD were listed. An important objective of this chapter has been to demonstrate some of these advantages, and what has been demonstrated is the ability of EPD to form thin layers and narrow lines of materials with controlled stoichiometry. However, there is much that can still be done in this area to present a convincing case for the industrial application of EPD.

A second major objective of this section has been to give examples of the full process of EPD including suspension development and post deposition processing. This allows the presentation several processes that can occur during the EPD of a powder material. These effects include: gravitational convection, ramified growth of metal deposits, density gradients in a deposition, very low density of deposits of non-conductive material by the direct electrostatic deposition, and the large compaction that can occur during drying. This section also highlights the importance of post deposition processing. Either by removing the deposition from the deposition electrode or by constrained sintering of the deposition on the substrate. This full cycle of pre-deposition processing, deposition, and post-deposition processing must be managed in the presence of various ancillary effects to begin to exploit the very real advantages of EPD for specific manufacturing tasks.

References

Chapter 5

1. Kumar, U., Wang, S.F., Selvaraj, U., and Dougherty, J.P., "Densification and Dielectric Properties of Hydrothermal $BaTiO_3$ with Different Sources of Bi_2O_3" *Ferroelectrics*, **154** (1994) 283-288

2. Pelton, R., Miller, P., McPhee, W., and Rajaram, S., "Strategies for Improving Electrophoresis Data from the Coulter DELSA", *Colloids and Surfaces A,* **80** (1993) 181-189

3. Lind, J.E. Jr., Zwolenik, J. J., and Fuoss, R. M., "Calibration of Conductance Cells at 25° with Aqueous Solutions of Potassium Chloride", *J. Am. Chem. Soc.* **81,** (1959) 1557-1559

4. Weidner, B. V., "The Conductivity of Electrolytes in Anhydrous Acetic Acid", Ph. D. Thesis, The Pennsylvania State University (1935)

5. Hunter, R. J., *Zeta Potential in Colloid Science, Principles and Applications*, Academic Press, New York, 1981

6. O'Brien, R. W., and White, L. R., "Electrophoretic Mobility of a Spherical Colloidal Particle", *J. Chem. Soc. Faraday II*, **74,** (1978) 1607

7. Loeb, A. L., Overbeek, J. Th. G., and Wiersma, P. H., *The Electrical Double Layer Around a Spherical Colloidal Particle*. MIT Press: Cambridge, Massachusetts, 1961

8. Russel, W.B., Saville, D.A. and Schowalter, W.R. , *Colloidal Dispersions,* Cambridge University Press, Cambridge, (1989)

9. Parsegian, V.A. and Weiss, G.H. "Spectroscopic Parameters for Computation of van der Waals Forces", *J. Colloid Interface Sci.* **81,** (1981) 285-289

10. Israelachvilli, J.N., *Intermolecular and Surface Forces*, Academic Press, New York (1992)

11. Van Tassel, J; Randall, CA, "Electrophoretic deposition and sintering of thin/thick PZT films" *J. Euro. Ceram. Soc.*, **19**[6-7] (1999) 955-958

12. Ogata, N; Van Tassel, J; Randall, CA, "Electrode formation by electrophoretic deposition of nanopowders" *Materials Letters,* **49**[1] (2001) 7-14

13. D. Stevens, and J. Gipprich, "Microwave Characterization and Modeling of Multilayered Cofired Ceramic Waveguides", *Intl. J. Microcircuits & Electronic Packaging*, **22**(1) (1999) 43

14. Setter, N.,"Electroceramics: looking ahead" *J. Euro. Ceram. Soc.*, **21**[10-11] (2001) 1279-1293

15. Whatmore, R.W., "Ferroelectrics, microsystems and nanotechnology", *Ferroelectrics*, **225**[1-4], (1999) 985-998

16. Janz, G.J., and Danyluk, S.S., "Conductances of Hydrogen Halides in Anhydrous Polar Organic Solvents", Chem. Rev., 60 (1960) 209-234

17. Tokuoka, Y., Kishi, T., and Nagai, T., "Electrophoretic Deposition of Nickel Ferrite Particles Dispersed in Acetone", *Denki Kagaku*, **42** (1974) 80-84
18. Northrip, J. W., “High Temperature Discharges in Ferroelectric Ceramics” *Journal of Applied Physics,* **31**[12] (1960) 2293-2296
19. F. Xu, F. Chu, and S. Trolier-McKinstry, "Longitudinal Piezoelectric Coefficient Measurement for Bulk Ceramics and Thin Films Using Pneumatic Pressure Rig," *J. Appl. Phys.*, **86**[1], (1999) 588 -594.
20. Randall C.A., Kim N., Kucera J.P., Cao W.W., Shrout T.R., "Intrinsic and extrinsic size effects in fine-grained morphotropic-phase-boundary lead zirconate titanate ceramics", *J. Am. Ceram. Soc.*, **81**[3] (1998) 677-688
21. M. J. Haun, Z. Q. Zhuang, E. Furman, Sei-Joo Jang, and L. E. Cross, “Electrostrictive Properties of the Lead Zirconate Titanate Solid Solution System”, *J. Am. Ceram. Soc.*, **72**[2], (1989) 1140-1144